

TULiP: Test-time Uncertainty Estimation via Linearization and Weight Perturbation

Yuhui Zhang¹, Dongshen Wu², Yuichiro Wada^{3,4}, and Takafumi Kanamori^{1,4}

¹ Institute of Science Tokyo, Japan kanamori@c.titech.ac.jp

² Imperial College London, UK

³ Fujitsu Limited, Japan

⁴ RIKEN AIP, Japan

Abstract. A reliable uncertainty estimation method is the foundation of many modern out-of-distribution (OOD) detectors, which are critical for safe deployments of deep learning models in the open world. In this work, we propose TULiP, a theoretically-driven post-hoc uncertainty estimator for OOD detection. Our approach considers a hypothetical perturbation applied to the network before convergence. Based on linearized training dynamics, we bound the effect of such perturbation, resulting in an uncertainty score computable by perturbing model parameters. Ultimately, our approach computes uncertainty from a set of sampled predictions. We visualize our bound on synthetic regression and classification datasets. Furthermore, we demonstrate the effectiveness of TULiP using large-scale OOD detection benchmarks for image classification. Our method exhibits state-of-the-art performance, particularly for near-distribution samples.

Keywords: Out-of-distribution detection · Neural Tangent Kernel .

1 Introduction

An important safety component for deep neural networks (NNs) in real-world environments is the awareness of their uncertainty upon receiving unknown or corrupted inputs. Such capability enables systems to fall back to conservative decision-making or defer to human judgments when faced with unfamiliar scenarios, which is imperative in safety-critical domains, such as autonomous driving [1] and medical applications [13]. The problem is often framed as **Out-Of-Distribution (OOD)** detection, which has witnessed significant growth in recent years [54].

Theoretically, this issue directly relates to quantifying epistemic uncertainty [24], which measures the lack of knowledge in a fitted model due to insufficient training data. The training process is typically modelled as a Bayesian optimization process [50] with approximations for practical use [15,8]. More generally, epistemic uncertainty could be formalized by the variance of a trained ensemble of networks $\phi(\mathbf{x}; \boldsymbol{\theta})$:

$$\text{Var}_{\boldsymbol{\theta}_{\text{init}}} [\phi(\mathbf{x}; \boldsymbol{\theta}_{\text{Train}})], \quad (1)$$

where θ_{Train} are parameters trained by some learning algorithm from random initialization θ_{Init} . Intuitively, higher prediction variance corresponds to inputs \mathbf{x} further from training set (OOD), as there lack enough training data to eliminate model disagreements via training, hence epistemic.

Many works redesign the network or training process to be uncertainty-aware [10,26]. However, these are often impractical due to heavy computational costs, especially for large datasets. Instead, *post-hoc* methods [38,39,20,11] are generally preferred. These approaches can be easily integrated into pre-trained models without interfering with the trained backbones, significantly enhancing their versatility [53]. Nevertheless, they often lack a direct theoretical link to the training process, which weakens their theoretical foundation and necessitates extensive empirical validation.

Therefore, it is desirable to develop a post-hoc OOD method with direct theoretical justifications regarding the training process. Recent analysis of NN optimizations reveals that gradient descent can be seen as its first-order approximations [28,36], termed *lazy* training, under specific conditions [16]. This enabled direct (but costly) computation of Eq. 1, as well as rigorous analysis [29] and methods [18] on model uncertainty, even beyond the lazy regime [6].

Inspired by this series of work, we present **TULiP** (**T**est-time **U**ncertainty by **L**inearized fluctuations via weight **P**erturbation), a post-hoc uncertainty estimator for OOD detection. Our method considers hypothetical fluctuations of the lazy training dynamics, which can be bounded under certain assumptions and efficiently estimated via weight perturbation. In practice, we found our method works well even beyond the ideal regime. Our contribution is threefold:

- (i) We provide a simple, versatile theoretical framework for analyzing epistemic uncertainty at inference time in the lazy regime, which is empirically verified;
- (ii) Based on our theory, we propose TULiP, an efficient and effective post-hoc OOD detector that does not require access to original training data;
- (iii) We test TULiP extensively using OpenOOD [56], a large, transparent, and unified OOD benchmark for image classifications. We show that TULiP consistently improves previous state-of-the-art methods across various settings.

The outline is as follows. Sec. 2 provides a summary of related works, Sec. 3 presents theoretical derivations, and Sec. 4 bridges theory to the implementation of TULiP. Sec. 5 reports the effectiveness of TULiP via empirical studies.

2 Related Works

Uncertainty Quantification (UQ) As being discussed in Sec. 1, theoretically-driven methods often estimates epistemic uncertainty from a Bayesian perspective. This includes, notably, Variational Inference [5]. Monte Carlo (MC) Dropout [15] connects Bayesian inference and the usage of Dropout layers, and is widely adopted in practice due to its simplicity and effectiveness. Moreover, Laplacian Approximation [8] approximates the posterior via Taylor expansion and Deep Ensembles [32] directly used independently trained deep models as an ensemble.

Post-hoc OOD Detectors For post-hoc methods, the baseline method using maximum softmax probability (MSP) was first introduced by [23]. ODIN [38] applies input preprocessing on top of temperature scaling [17] to enhance MSP. [39] proposes a simple score based on energy function (EBO). [20] uses maximum logits (MLS) for efficient detection on large datasets. GEN [40] adopts the generalization of Shannon Entropy, while ASH [11] prunes away samples' activation at later layers and simplifies the rest. Some methods also access the training set for additional information, as MDS [37] used Mahalanobis distance with class-conditional Gaussian distributions, and ViM [52] computes the norm of the feature residual on the principal subspace for OOD detection.

Due to the nature of post-hoc setting, most methods such as EBO, ODIN and MLS compute OOD score solely from trained models, overlooking the training process. In contrast, as previously stated, inspired by the more theoretically-aligned UQ methods, TULiP addresses the problem with regard to the training process from a theoretical aspect. In practice, TULiP works by a series of carefully constructed weight perturbations, ultimately yielding a set of model predictions, which can be seen as surrogates to posterior samples for OOD detections. Our contribution is orthogonal to methods working with logits and predictive probabilities, such as GEN, as they can work on top of TULiP outputs. In such an aspect, TULiP shares the similar plug-and-play versatility as seen in recent works, such as ReAct [45] and RankFeat [44].

3 Theoretical Framework

3.1 Preliminaries: Linearized Training Dynamics

Theories involving Neural Tangent Kernel (NTK) consider the linearization of neural networks. It has been shown that under an infinite width (lazy) limit, network parameters and hence the gradients barely change across the whole training process, justifying the linearization of the training process [28]. [36] extends the result by examining them in the parameter space, with a formal result equalizing linearized networks and empirical ones under mild assumptions.

Let $f_{\text{True}}(\mathbf{x}; \boldsymbol{\theta}) : \mathbb{R}^d \rightarrow \mathbb{R}^o$ be a neural network parameterized by parameters $\boldsymbol{\theta}$. We write the Jacobian (gradient) evaluated at \mathbf{x} as $\nabla_{\boldsymbol{\theta}} f_{\text{True}}(\mathbf{x}) \in \mathbb{R}^{o \times |\boldsymbol{\theta}|}$, where $|\boldsymbol{\theta}|$ is the cardinality of $\boldsymbol{\theta}$, i.e., the number of parameters in the network.

Let $f(\mathbf{x}; \boldsymbol{\theta})$ denote the network linearized at $\boldsymbol{\theta}^*$:

$$f(\mathbf{x}; \boldsymbol{\theta}) := f_{\text{Init}}(\mathbf{x}) + \nabla_{\boldsymbol{\theta}} f_{\text{True}}(\mathbf{x})|_{\boldsymbol{\theta}=\boldsymbol{\theta}^*} (\boldsymbol{\theta} - \boldsymbol{\theta}^*), \quad (2)$$

where $f_{\text{Init}}(\mathbf{x})$ is the initial network function. Here, we treat it as a linear approximation to the true training dynamics. For our convenience, we will interchangeably use $\nabla_{\boldsymbol{\theta}} f(\mathbf{x})$ as $\nabla_{\boldsymbol{\theta}} f_{\text{True}}(\mathbf{x})|_{\boldsymbol{\theta}=\boldsymbol{\theta}^*}$.

We consider the training data \mathbf{x} within an empirical dataset X . For a twice-differentiable loss function $\ell(f(\mathbf{x}); y(\mathbf{x}))$ with target $y(\mathbf{x})$, we write it's gradient w.r.t. $f(\mathbf{x})$ as $\ell'(f(\mathbf{x}); y(\mathbf{x}))$ (or simply $\ell'(f(\mathbf{x}))$). Then, following [36], f is trained on X following the gradient flow:

$$\partial_t f_t(\mathbf{x}) = -\eta \mathbb{E}_{\mathbf{x}'} [\Theta(\mathbf{x}, \mathbf{x}') \ell'(f_t(\mathbf{x}'); y(\mathbf{x}'))], \quad (3)$$

where $\mathbb{E}_{\mathbf{x}'}$ is the expectation w.r.t. the empirical distribution for $\mathbf{x}' \in X$, η is the learning rate and f_t denotes the network f at time $t \in [0, T]$. Given inputs \mathbf{x}, \mathbf{x}' , the NTK $\Theta(\mathbf{x}, \mathbf{x}') \in \mathbb{R}^{o \times o}$ defined as $\Theta(\mathbf{x}, \mathbf{x}') := \nabla_{\boldsymbol{\theta}} f(\mathbf{x}) \nabla_{\boldsymbol{\theta}} f(\mathbf{x}')^\top$ governs the linearized training Eq. 3. Under the lazy limit, the NTK $\Theta(\mathbf{x}, \mathbf{x}')$ stays constant across the training process and hence is independent of t . Hereon, we assume the unique existence of the solution to Eq. 3.

Notations Let $\mathbf{z} \in \mathbb{R}^d$ be an arbitrary test point. Let $\|\cdot\|$ denote the Euclidean norm and induced 2-norm for vectors and matrices. Let $\|\cdot\|_F$ denote the matrix Frobenius norm. We also denote $\|\cdot\|_X := \mathbb{E}_{\mathbf{x}} [\|\cdot\|^2]^{1/2}$ the data-dependent norm through out the following descriptions. For a matrix \mathbf{A} , let $|\mathbf{A}|$ be the unique symmetric positive semi-definite solution of $|\mathbf{A}|^2 = \mathbf{A}^\top \mathbf{A}$. It is an extension of absolute values to matrices. Finally, let $f(\mathbf{z}) \lesssim g(\mathbf{z})$ indicate $f(\mathbf{z}) \leq g(\mathbf{z}) + M$ up to some constant M independent of \mathbf{z} .

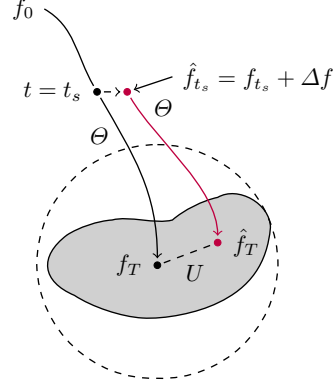


Fig. 1: Illustration of the hypothetical perturbation process. The shaded area indicates the distribution of \hat{f}_T , and the dashed circle is the Surrogate Posterior Envelope (SPE). See Sec. 4.3 for details.

3.2 Modeling Uncertainty

Under our problem setting, neither the distribution of initialized models nor the training process is accessible, which renders a significant difficulty for the direct computation of the uncertainty shown in Eq. 1. Instead, we choose to intuitively model it by considering a perturbation applied towards the network function $f(\mathbf{x})$, at a time $t = t_s$ before the training terminates at $t = T$. It is important to note that, this perturbation prior to convergence is *hypothetical*, as it is inaccessible in our post-hoc setting, and we will only use it to establish our theoretical framework.

Formally, consider a perturbation to f_{t_s} at $t = t_s$ as $\hat{f}_{t_s}(\mathbf{x}) = f_{t_s}(\mathbf{x}) + \Delta f(\mathbf{x})$. After the perturbation, the perturbed network $\hat{f}(\mathbf{x})$ will be trained following the same dynamics as Eq. 3:

$$\partial_t \hat{f}_t(\mathbf{x}) = -\eta \mathbb{E}_{\mathbf{x}'} [\Theta(\mathbf{x}, \mathbf{x}') \ell'(\hat{f}_t(\mathbf{x}'); y(\mathbf{x}'))], \quad (4)$$

until termination time T .

Under such a perturb-then-train process, we model the epistemic uncertainty U as the difference between converged networks, reads $\|f_T(\mathbf{z}) - \hat{f}_T(\mathbf{z})\|$, as illustrated in Fig. 1. It measures the fluctuation of the training process, capturing the sensitivity of training w.r.t. noise. Indeed, by applying a perturbation at $t = 0$, we essentially perturb f_{init} , which can be seen as a sampling process from some model prior (Appendix A.7). In this case, $\hat{f}_T(\mathbf{z})$ can be interpreted

as samples from the trained ensemble as in Eq. 1, where their variance reflects epistemic uncertainty.

However, as stated above, in practice we only know the trained network f_T at $t = T$. It would be impractical to recover the full training trajectory, apply the perturbation at $t = t_s$ and then retrain the network. Therefore, in the following, we will come up with a bound of $\|f_T(\mathbf{z}) - \hat{f}_T(\mathbf{z})\|$ given the strength of the perturbation Δf , which can be evaluated at \mathbf{z} without actually retrain the network. Thus, the perturbation is *hypothetical*, as it has never been applied in our practice.

3.3 Bounding Linearized Training Fluctuations

To present the bound, we shall introduce the following assumptions:

- A1. (**Boundedness**) For $t \in [0, T]$, $f(\mathbf{x})$, $\nabla_{\boldsymbol{\theta}} f(\mathbf{x})$, ℓ and ℓ' stay bounded, uniformly on \mathbf{x} .
- A2. (**Smoothness**) Gradient ℓ' of loss function ℓ is Lipschitz continuous: $\forall \mathbf{x} \in X$; $\|\ell'(\hat{\mathbf{y}}; y(\mathbf{x})) - \ell'(\hat{\mathbf{y}}'; y(\mathbf{x}))\| \leq L\|\hat{\mathbf{y}} - \hat{\mathbf{y}}'\|$.
- A3. (**Perturbation**) The perturbation Δf can be uniformly bounded by a constant α , that is, for all \mathbf{x} (not limited to the support of training data), i.e., $\forall \mathbf{x} \in \mathbb{R}^d$; $\|\Delta f(\mathbf{x})\| \leq \alpha$.
- A4. (**Convergence**) Most importantly, for the original network trained via Eq. 3 and the perturbed network trained via Eq. 4, we assume *near-perfect convergence* on the training set \mathbf{x} at termination time $t = T$, i.e., $\exists \beta \in \mathbb{R}, \forall \mathbf{x} \in X$; $\|f_T(\mathbf{x}) - \hat{f}_T(\mathbf{x})\| \leq \beta$.
- A5. (**Closeness**) The test point \mathbf{z} is close to the training set X in the sense that $\inf_{\mathbf{x} \in X} \|\nabla_{\boldsymbol{\theta}} f(\mathbf{z}) - \nabla_{\boldsymbol{\theta}} f(\mathbf{x})\|_{\text{F}}^2 \leq \text{Tr}(\Theta(\mathbf{z}, \mathbf{z}) + \mathbb{E}_{\mathbf{x}}[\Theta(\mathbf{x}, \mathbf{x})] - 2\mathbb{E}_{\mathbf{x}}[\Theta(\mathbf{z}, \mathbf{x})])$.

Under reasonable conditions, it has been shown both empirically [55] and theoretically [12] that overparameterized NNs trained via SGD is able to achieve near-zero training loss on almost arbitrary training sets. To nice loss functions as $\ell(\mathbf{y}; \mathbf{y}') = 0$ implies $\mathbf{y} = \mathbf{y}'$, this implies A4.

We note that the closeness assumption A5 is weak. Intuitively, it assumes that for $\mathbf{x} \in X$, $\Theta(\mathbf{z}, \mathbf{x})$ contains many positive singular values (\mathbf{z} is close to \mathbf{x} in the sense of Θ). Fig. 2(c) provides empirical justifications for this closeness assumption.

[28] connected lazy NNs trained with mean square error (MSE) loss and kernel ridge regression. Essentially, it hints that under such a setup, an NN embeds datapoints \mathbf{x} into gradients $\nabla_{\boldsymbol{\theta}} f(\mathbf{x})$. Indeed, for a general class of loss functions, it is possible to show that:

Theorem 1. *Under assumptions A1-A4, for a network f trained with Eq. 3 and a perturbed network \hat{f} trained with Eq. 4, the perturbation applied at time $t_s = T - \Delta T$ bounded by α , we have*

$$\|f_T(\mathbf{z}) - \hat{f}_T(\mathbf{z})\| \leq \inf_{\mathbf{x} \in X} C \|\nabla_{\boldsymbol{\theta}} f(\mathbf{z}) - \nabla_{\boldsymbol{\theta}} f(\mathbf{x})\|_{\text{F}} + 2\alpha + \beta, \quad (5)$$

where $C = \frac{\alpha\eta\bar{\Theta}_X^{1/2}}{\lambda_{max}} (e^{(T-t_s)L\lambda_{max}} - 1)$, $\bar{\Theta}_X^{1/2} := \|\nabla_{\theta} f(\mathbf{x})\|_X$ is average gradient norm over training data, and $\lambda_{max} := \frac{1}{\sqrt{N}}\|\mathbf{G}\|$ for a generalized Gram matrix $G_{i,j} := \|\Theta(x_i, x_j)\|$ of dataset $X = \{x_1, x_2, \dots, x_N\}$.

Furthermore, under assumption A5, up to constants J and K ,

$$\|f_T(\mathbf{z}) - \hat{f}_T(\mathbf{z})\| \lesssim J \left[\text{Tr}(\Theta(\mathbf{z}, \mathbf{z}) + \mathbb{E}_x[\Theta(\mathbf{x}, \mathbf{x})]) - 2K \|\nabla_{\theta} f_T(\mathbf{z})\| \|\boldsymbol{\theta}_T - \boldsymbol{\theta}_{t_s}\| \right]^{\frac{1}{2}}. \quad (6)$$

Proof. With an arbitrarily chosen pivot point \mathbf{x}^* from the training set, it is possible to bound $\|f(\mathbf{z}) - f(\mathbf{x}^*)\|$ and $\|\hat{f}(\mathbf{z}) - \hat{f}(\mathbf{x}^*)\|$ by bounding the fluctuations on the training set. Eq. 5 then follows from assumption A4. Combine A5, linearized training and Hölder’s inequality, we derive Eq. 6. Please check Sec. A.3 for details.

We see that the bound Eq. 5 on the training fluctuation is dominated by the distance from test point \mathbf{z} to the training set X in the “embedding space” of gradients. It is then possible to obtain a bound on such a distance using trained network parameters as in Eq. 6. A key insight here is that the gradient information during the training process has been accumulated into the trained weights.

Network Ensemble We close this section by the fact that

$$\text{Tr}(\text{Var}_{\Delta f}[\hat{f}_T(\mathbf{z})]) \leq \mathbb{E}_{\Delta f}[\|\hat{f}_T(\mathbf{z}) - f_T(\mathbf{z})\|^2], \quad (7)$$

which can be then bounded by Eq. 6. As we stated before, $\hat{f}_T(\mathbf{z})$ can be seen as samples from the trained ensemble as in Eq. 1. In practice, it is often beneficial to obtain such samples. In the next section, we will present a heuristic method to estimate $\hat{f}_T(\mathbf{z})$ by matching variances.

4 Implementation

In this section, we present the key implementation strategies that enhance the practical effectiveness of our method, TULiP, summarized in Alg. 1. We elaborate on its design in the following subsections by referring to lines in Alg. 1.

In contrast to the linearized network $f(\mathbf{x}; \boldsymbol{\theta})$, let $f_t^{emp}(\mathbf{x}; \boldsymbol{\theta})$ denote a network trained empirically. Intuitively, trajectories of $f_t(\mathbf{x}; \boldsymbol{\theta})$ and $f_t^{emp}(\mathbf{x}; \boldsymbol{\theta})$ is similar when $\boldsymbol{\theta}^* = \boldsymbol{\theta}_{\text{Init}}$ with a small learning-rate [36,16]. Under a post-hoc setting, as only converged models are available, we take $t_s = 0$ and substitute $\boldsymbol{\theta}_{t_s}$ with $\mathbb{E}[\boldsymbol{\theta}_0] = \mathbf{0}$ (or other mean specified by initialization schemes, e.g., $\mathbb{E}[\gamma_0] = \mathbf{1}$ in BatchNorm layers) in our implementation. We also use the empirical NTK $\tilde{\Theta}_T^{emp}$ at convergence time as an approximation for the kernel Θ used in Eq. 3:

$$\tilde{\Theta}_T^{emp}(\mathbf{z}, \mathbf{x}) := \nabla_{\theta} f_T^{emp}(\mathbf{z}) \nabla_{\theta} f_T^{emp}(\mathbf{x})^{\top} \approx \Theta(\mathbf{z}, \mathbf{x}), \quad (8)$$

We first introduce how we estimate Eq. 6 using f_T^{emp} at $t = T$. Then, we introduce the construction of surrogate posterior samples that greatly enhance our method.

Algorithm 1 TULiP for Classifiers.

Input: Input $z \in \mathbb{R}^d$, trained parameters θ_T , network $f^{emp}(z; \theta) : \mathbb{R}^d \rightarrow \mathbb{R}^o$
Parameter: Calibrated parameters J, Θ_{XX} ; Perturbation strength ϵ, δ ; Parameter λ ;
 Number of posterior samples M
Output: Uncertainty score U

```

1:  $\theta_{t_s} \leftarrow \mathbb{E}\theta_0$ 
2: for  $i = 1, \dots, M$  do
3:   Sample  $v_i \in \mathbb{R}^{|\theta|}$  from  $\mathcal{N}(0, \epsilon^2 \mathbf{I})$ 
4:    $\tilde{f}_i^{raw}(z) \leftarrow f^{emp}(z; \theta_T + v_i)$ 
5: end for
6:  $\tilde{\Theta}_{Tr}(z, z) \leftarrow \frac{1}{M} \sum_i \|\tilde{f}_i^{raw}(z) - f^{emp}(z; \theta_T)\|^2$  ▷ Estimation of  $\text{Tr } \Theta(z, z)$ 
7:  $D \leftarrow \sqrt{o} \|f^{emp}(z; \theta_T + \epsilon\delta(\theta_T - \theta_{t_s})) - f^{emp}(z; \theta_T)\|$ 
8:  $S \leftarrow J^2 \cdot \left( \tilde{\Theta}_{Tr}(z, z) + \Theta_{XX} - \lambda D \right)$  ▷ Estimation of Eq. 6 up to square root
9:  $\gamma \leftarrow \sqrt{\max(S, 0) / \tilde{\Theta}_{Tr}(z, z)}$ 
10: for  $i = 1, \dots, M$  do ▷ Surrogate posterior samples
11:    $\tilde{f}_i(z) \leftarrow (1 - \gamma)f^{emp}(z; \theta_T) + \gamma\tilde{f}_i^{raw}(z)$ 
12: end for
13:  $U \leftarrow \mathbb{H}_y(\frac{1}{M} \sum_i \text{softmax}(\tilde{f}_i(z)))$ 

```

4.1 Estimation of Jacobian (Line 2 - 8)

Estimating gradients explicitly is both time and memory-consuming, especially for networks with large output dimensions. Fortunately, Eq. 6 only contains z -dependent terms that can be computed via perturbations on model weights θ . Namely, for $\|\nabla_{\theta} f_T(z) (\theta_T - \theta_{t_s})\|$:

$$\lim_{\delta \rightarrow 0} \frac{1}{\delta} (f^{emp}(z; \theta_T + \delta(\theta_T - \theta_{t_s})) - f^{emp}(z; \theta_T)) \approx \nabla_{\theta} f_T(z) (\theta_T - \theta_{t_s}) \quad (9)$$

is used in line 7 of Alg. 1, corresponds to a deterministic perturbation. The additional \sqrt{o} scaling arises naturally in the derivation of Thm. 1.

For $\text{Tr } \Theta(z, z)$, we could estimate its value with Hutchinson's Trace Estimator [2] (line 2-6), corresponds to a Gaussian perturbation (noise) on θ .

Proposition 1. Suppose that f^{emp} is γ -smooth w.r.t. θ , i.e.,

$$\|\nabla_{\theta} f^{emp}(z; \theta) - \nabla_{\theta} f^{emp}(z; \theta')\|_F \leq \gamma \|\theta - \theta'\|.$$

Let \mathbf{v} be a random variable such that $\mathbb{E}_{\mathbf{v}}[\mathbf{v}] = \mathbf{0}$, $\mathbb{E}_{\mathbf{v}}[\mathbf{v}\mathbf{v}^\top] = \epsilon^2 \mathbf{I}$ and $\mathbb{E}_{\mathbf{v}}[\|\mathbf{v}\|^k] \leq C_k \epsilon^k$ for $k = 3, 4$, where C_k is a constant depending on k and the dimension of \mathbf{v} . Then, under A1, it holds that

$$\lim_{\epsilon \rightarrow 0} \frac{1}{\epsilon^2} \mathbb{E}_{\mathbf{v}} [\|f^{emp}(z; \theta_T + \mathbf{v}) - f^{emp}(z; \theta_T)\|^2] = \text{Tr} \left(\tilde{\Theta}_T^{emp}(z, z) \right). \quad (10)$$

Note that the multi-dimensional normal distribution with mean zero and variance-covariance matrix $\epsilon^2 \mathbf{I}$ agrees to the condition of \mathbf{v} . Prop. 1 and the approximation Eq. 8 ensures that $\text{Tr } \Theta(z, z)$ is approximated by $\epsilon^{-2} \mathbb{E}_{\mathbf{v}} [\|f^{emp}(z; \theta_T + \mathbf{v}) - f^{emp}(z; \theta_T)\|^2]$ with a small ϵ .

Proof. Please check Sec. A.5 for details.

From above, \mathbf{z} -relevant terms in Eq. 6 can be approximated while avoiding explicit computation of $\nabla_{\boldsymbol{\theta}} f(\mathbf{z})$. Specifically, in line 8, S provides an estimation of the upper-bound Eq. 6 up to $\mathbb{E}_{\mathbf{x}}[\Theta(\mathbf{x}, \mathbf{x})]$, square root and constants. Here, the hyper-parameter λ acts as a proxy to the constant K . Such approximation is implemented by perturbations to $\boldsymbol{\theta}$, thus compatible with mini-batching, enabling fast computation with $\mathcal{O}(M)$ forward passes.

4.2 Calibration on Validation Dataset

In practice, a validation dataset X_{Val} of ID data is often available to produce reliable results [56]. Such data is valuable in finding optimal J and $\mathbb{E}_{\mathbf{x} \sim P_X}[\Theta(\mathbf{x}, \mathbf{x})]$.

$\mathbb{E}_{\mathbf{x} \sim P_X}[\Theta(\mathbf{x}, \mathbf{x})]$ can be estimated straight-forwardly by using the empirical expectation on X_{Val} . To find J , we first construct $\tilde{f}_i(\mathbf{z})$ on $\mathbf{z} \in X_{\text{Val}}$ following the step shown in Alg. 1 (line 1-11) with chosen ϵ, λ and $J = 1$. $\tilde{f}_i(\mathbf{z})$ for varying J s can be easily obtained by controlling the scaling factor γ . Therefore, we find the optimal non-negative J^* by maximizing the likelihood of $\frac{1}{M} \sum_i \text{softmax}(\tilde{f}_i(\mathbf{z}))$ over $\mathbf{z} \in X_{\text{Val}}$.

For OOD detection however, we empirically found that a bigger J sometimes gives better results. Therefore, we set $J = J_{\text{scaling}} \cdot J^*$ with hyper-parameter $J_{\text{scaling}} \geq 1$ in practice.

4.3 Surrogate Posterior Envelope (SPE) (Line 9 - 13)

Many OOD detection methods work with the predictions produced by a neural network [54]. As shown later in Table 1, a sufficiently trained model’s raw prediction output (MSP) is already a robust OOD estimator. Such OOD detection capability can be combined with Thm. 1 to further improve TULiP’s performance.

Intuitively, a well-trained classifier can be certain that a test datum \mathbf{z} belongs to neither class, in the sense that an evaluation of Eq. 6 yields a small value, but its prediction $\text{softmax}(f_T(\mathbf{z}))$ indicates OOD input (i.e., it belongs to neither class). To this end, borrowing ideas from the Model Averaging literature [15,32], we propose to use the averaged prediction of the *hypothetically-perturbed-then-trained* models $\mathbb{E}_{\Delta f}[\text{softmax}(\hat{f}(\mathbf{z}))]$ for OOD detection.

The distribution of $\hat{f}(\mathbf{x})$ is intractable without access to the training process. Fortunately, we may approximate it via the bound Eq. 6 by constructing an envelope around the true distribution, as depicted in Fig. 1. From line 11, it is possible to show

$$\text{Tr}(\text{Var}_i[\tilde{f}_i(\mathbf{z})]) \approx \gamma^2 \cdot \text{Tr}(\text{Var}_i[\tilde{f}_i^{\text{raw}}(\mathbf{z})]) = S, \quad (11)$$

for a positive S and small ϵ such that $\mathbb{E}_i[\tilde{f}_i^{\text{raw}}(\mathbf{z})] \approx f^{\text{emp}}(\mathbf{z}; \boldsymbol{\theta}_T)$. Note that γ is given in line 9 of Alg. 1, and S is an estimate of Eq. 6 as stated in the previous subsection. Sec. A.6 provides additional derivations to clarify their relationships.

For classification problems, after obtaining $\mathbf{v} := \mathbb{E}_{\Delta f}[\text{softmax}(\hat{f}(\mathbf{z}))]$, TULiP applies the information entropy $\mathbb{H}_y[\mathbf{v}] := -\sum_{y=1}^o \mathbf{v}_y \log \mathbf{v}_y$ to produce OOD score

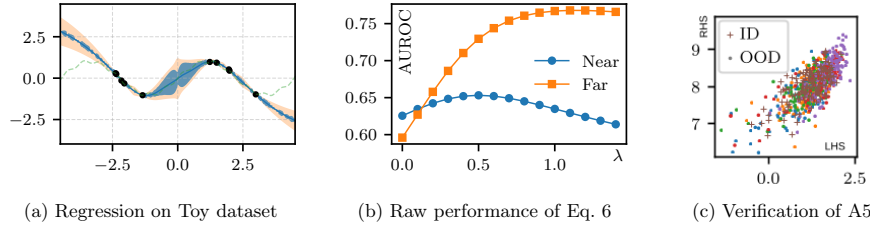


Fig. 2: Verification of Thm. 1 (Sec. 5.1). From left to right, (a): Regression on Splines. Light shade: the bound Eq. 5, heavy shade: Ground-truth ensemble (Eq. 1), black dots: training data. (b): OOD Detection capability of Eq. 6 on ImageNet-1K setup, using S in Alg. 1 (line 13, used to estimate Eq. 6) as OOD scoring function. (c): Verification of A5 on ImageNet-1K setup.

as shown in line 13 of Alg. 1. Other methods, such as GEN [40], can also be naturally incorporated into TULiP.

Alg. 1 summarizes TULiP, our proposed uncertainty estimator for OOD detection. Although Alg. 1 gives TULiP for classification, it naturally generalizes to non-classification problems as TULiP constructs surrogate posterior samples. In practice, TULiP can be accessed via: 1) Obtain the trained model on ID dataset, 2) Calibrate J and Θ_{XX} on a small validation dataset and 3) Apply Alg. 1 on test data.

5 Experiments

A key assumption of TULiP is linearized training. However, it raises practical concerns, as empirical deep networks are typically trained non-linearly [14]. In this section, we demonstrate that TULiP nevertheless works under practical setups, by investigating TULiP in OOD tasks and comparing it with state-of-the-art OOD detectors.

Experiment Setup We evaluate the practical performance of TULiP with OOD detection tasks based on manually defined ID-OOD dataset pairs, following the OpenOOD v1.5 benchmark [56]. OOD data range across a collection of diverse image datasets, categorized into *near* and *far* OOD sets [53], where near is more similar to ID and therefore more difficult to distinguish. Following their setup, we use the same pre-trained ResNet-18 [19] for CIFAR-10 & 100 [30] and ImageNet-200 [56] ID datasets, and ResNet-50 for ImageNet-1K [43].

For TULiP, we use $M = 10$ surrogate posterior samples with $\epsilon = 0.005$, $\delta = 8$ and $\lambda = 1.25$. We perturb all available parameters in the network including biases and Batch Normalization parameters β, γ [27]. Following [56], we conduct a hyper-parameter search on a small validation set whenever possible, within a reasonable range of $J_{\text{scaling}} \in \{1.0, 1.25, 1.5, 1.75, 2.0\}$. We explain our choice for hyper-parameters in Sec. B.2. We present details of all datasets in Sec. B.1.

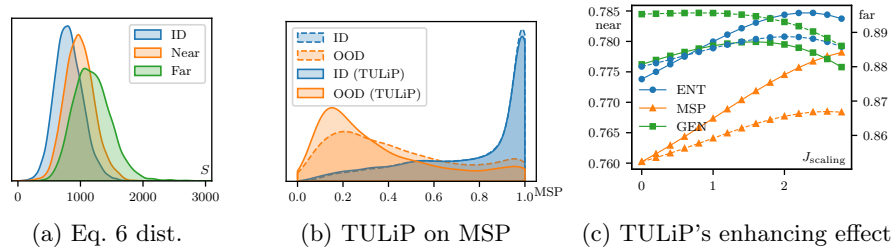


Fig. 3: (a) Visualization of S in Alg. 1 (line 13, used to estimate Eq. 6) in various datasets (left to right: ID (ImageNet-1K), NINCO (near), Textures (far)). (b) Visualization of the MSP score before and after applying TULiP on ID (right) and OOD (left). Notice how OOD data is pushed further towards 0 (lower confidence) than ID. We chose MSP due to its simplicity. (c) Effect of TULiP on various OOD scoring criteria for near-OOD (solid) and far-OOD (dashed). J_{scaling} (horizontal axis) controls the strength of TULiP, where a value of 0 indicates baselines without TULiP.

5.1 Empirical Validation for Section 3

Synthetic Datasets We begin by validating the original bound presented in Eq. 5 using toy regression data. A 3-layer infinite-wide feed-forward neural network is used, and we solved the lazy training dynamics over the dataset using the *neural-tangents* library [42]. We used MSE loss and computed the exact Gaussian ensemble [36]. Results are shown in Fig. 2(a). It suggests that our bound Eq. 5 based on training fluctuations is able to capture the true epistemic uncertainty as in Eq. 1, justifies further developments of our method.

Eq. 6 in Practice We further validate the proposed bound Eq. 6 by its OOD detection performance in practical scenarios. Using the ImageNet-1K setup, Fig. 2(b) shows the positive OOD detection capability of Eq. 6. In practice, it is estimated using S in Alg. 1 (line 13).

By setting $\lambda = 0$, we effectively recover an OOD scoring criteria similar to GradNorm [25]. GradNorm computes the OOD score based on the gradient of KL divergence between softmax-ed prediction and a uniform distribution, where ID data is claimed to have larger gradient compared to OOD data. In contrast, our OOD score in Fig. 2(b) (when $\lambda = 0$), is computed from the Frobenius norm of gradient of *logits* w.r.t. network parameters evaluated at given input. In logit space, it is shown that the OOD data instead have a slight *larger* gradient compared to the ID data (Fig. 2(b), when $\lambda = 0$, AUROC > 0.5 indicates that the OOD data have larger gradients on average).

Furthermore, the performance of Eq. 6 is boosted when using a positive λ , supports our claim that the parameter-gradient product $\|\nabla_{\theta} f_T(\mathbf{z})(\theta_T - \theta_{t_s})\|$ provides useful information of training dataset as Thm. 1 suggested. Especially in the *far-OOD* split, such performance boost of the λ -term is surprisingly significant

Table 1: Results on OpenOOD benchmark, averaged from 3 runs. The top results for each category are marked in bold, with the second-best result in underlined. We include baseline results from [56], and reproduced the results for MC-Dropout (MCD). A dagger symbol † indicates direct access to training data or processes. Results are averaged separately for *near* / *far*-OOD sets.

Method	CIFAR-10		CIFAR-100		ImageNet-200		ImageNet-1K	
	FPR@95 ↓	AUROC ↑	FPR@95 ↓	AUROC ↑	FPR@95 ↓	AUROC ↑	FPR@95 ↓	AUROC ↑
MCD †	53.54/31.43	87.68/91.00	<u>54.73</u> /59.08	80.42/77.58	55.25/35.48	83.30/90.20	65.68/51.45	76.02/85.23
MDS †	49.90/32.22	84.20/89.72	83.53/72.26	58.69/69.39	79.11/61.66	61.93/74.72	85.45/62.92	55.44/74.25
ViM †	<u>44.84</u> / 25.05	<u>88.68</u> / 93.48	62.63/ 50.74	74.98/ 81.70	59.19/ 27.20	78.68/91.26	71.35/ <u>24.67</u>	72.08/92.68
MSP	48.17/31.72	88.03/90.73	54.80/58.70	80.27/77.76	<u>54.82</u> /35.43	83.34/90.13	65.68/51.45	76.02/85.23
ODIN	76.19/57.62	82.87/87.96	57.91/58.86	79.90/79.28	66.76/34.23	80.27/91.71	72.50/43.96	74.75/89.47
MLS	61.32/41.68	87.52/91.10	55.47/56.73	<u>81.05</u> /79.67	59.76/34.03	82.90/91.11	51.35 /63.60	76.46/89.57
ASH	86.78/79.03	75.27/78.49	65.71/59.20	78.20/ <u>80.58</u>	64.89/ <u>27.29</u>	82.38/ 93.90	<u>63.32</u> / 19.49	<u>78.17</u> / 95.74
GEN	53.67/47.03	88.20/91.35	54.42 /56.71	81.31 /79.68	55.20/32.10	<u>83.68</u> /91.36	65.32/35.61	76.85/89.76
EBO	61.34/41.69	87.58/91.21	55.62/56.59	80.91/79.77	60.24/34.86	82.50/90.86	68.56/38.39	75.89/89.47
ENT	48.17/31.71	88.12/90.84	54.81/58.69	80.63/78.14	<u>54.82</u> /35.34	83.55/90.52	65.63/51.28	76.55/86.21
ReAct (EBO)	63.56/44.90	87.11/90.42	56.39/ <u>54.20</u>	80.77/80.39	62.49/28.50	81.87/ <u>92.31</u>	66.69/26.31	77.38/93.67
TULiP (ENT)	40.77 / <u>28.40</u>	89.36 / <u>92.25</u>	56.21/57.94	80.81/78.75	54.75 /33.62	83.84 /91.05	64.96/48.01	78.38 /88.85

(improved AUROC over 15%). *Far-OOD* contains images that are different from ID more significantly. It could potentially be an easy case for Eq. 6, in the sense that a relatively looser bound (as having no access to training data), especially $\|\nabla_{\theta} f_T(\mathbf{z})(\theta_T - \theta_{t_s})\|$, can still retrieve enough training information for OOD detection, as discussed in Sec. 3.3. Note that despite being far, *far-OOD* data still satisfy the closeness assumption A5 as shown in Fig. 2(c).

5.2 Out-of-distribution Detection

Baseline Methods Shannon Entropy (ENT) computes the entropy of plain network prediction. ENT is an important baseline, as TULiP works by providing it with TULiP-enhanced predictions (average from SPE). We also consider various baselines other than ENT for comparison, including the MC-Dropout (MCD), post-hoc OOD methods without training data ODIN, EBO, MLS, ASH and GEN; and finally, MDS and ViM with access to training data. Please refer to Sec. 2 for a brief introduction.

Results We report the performance of TULiP on OpenOOD v1.5 benchmark [56] in Table 1. TULiP consistently improves over the ENT on both near- and far-OOD setups. It achieves remarkable performance in near-OOD settings with either top-1 or top-2 AUROC scores across all datasets, and is on par with most methods in far-OOD settings. It is essential to note that methods that significantly outperform TULiP on far-OOD either access the training dataset (ViM and MDS) or completely lack a theoretical explanation (ASH). As we discuss below, TULiP is also more consistent compared to other methods such as ASH.

Table 2: Extended results on ImageNet-1K (in AUROC \uparrow). Some baseline results cited from [56]. Evaluating ASH on OpenOOD framework [53] with unsupported network architectures (MobileNet, VGG-16, RegNet) is difficult and thus omitted.

Method	ResNet-50(V2)	ViT-16-B	MobileNet-V3-Large	VGG-16	RegNet-Y-16GF
EBO	54.39/51.36	62.41/78.98	71.00/77.46	72.16/89.92	67.50/69.98
ODIN	69.89/66.10	64.32/76.06	70.09/79.63	70.86/90.83	64.93/65.41
MLS	69.24/76.47	68.30/83.54	74.39/82.67	72.75/89.78	72.07/78.45
ASH	35.96/29.91	53.21/51.56	-/-	-/-	-/-
TULiP	66.77/74.35	72.96/87.42	75.20/84.40	74.54/87.51	74.54/83.52

Consistency To further validate the consistency of TULiP, we conduct ImageNet-1K OOD experiments with various network architectures and training protocol, using pretrained models available online [?]. We report the results in Table 2. TULiP consistently achieves top-class performance across various setups. Notably, ASH fails when ResNet-50(V2) weights are used. V2 weights are trained with recent advances in practical NN training, increasing the Top-1 accuracy by 4.7% [?]. Such a complicated training process may render difficulties when applying methods like ASH without theoretical guidance.

TULiP Enhancing Baseline Methods The proposed algorithm Alg. 1 works with Shannon Entropy to compute an OOD score from averaged predictions. Such choice is due to the superior performance of the entropy score when paired with TULiP, as shown in Table 1. Indeed, other methods can also work with TULiP’s averaged prediction, as TULiP enhances their performance on OOD tasks. We demonstrate such an enhancing effect using MSP score (i.e., raw confidence of predicted class) in Fig. 3(b), using ImageNet-1K (ID) and Textures (OOD). With weight perturbations, TULiP pushes original network predictions towards a more uniform distribution, with an increased effect particularly on OOD data. We compare the enhancing effect of various methods in Fig. 3(c).

ReAct [46] is similar to TULiP as an enhancement method (in this case, over EBO), while TULiP provides a more consistent improvement in all datasets. TULiP can also be combined with ReAct as they operate on different aspects of a network, yet the details of such a combination need further investigation.

Ablation Study and Hyper-parameters We conduct experiments on ImageNet-1K to analyze the effect and consistency of hyper-parameters. The results are shown in Fig. 4, where we observe a consistent behavior of the parameter λ in near- and far-OOD setups. Given a fixed ϵ , the optimal λ for near- and far-OOD setups is similar, simplifies the hyper-parameter tuning process. It also further validates the positive effect of the λ -term in TULiP for OOD detection. As shown in Fig. 4, a slight larger ϵ can also increase the stability of TULiP w.r.t. changes in λ , where larger ϵ favors larger λ (also corresponds to smaller J^*). In practice, the calibration step of finding an optimal J ensures consistent performance across various setups, as shown in Fig. 4 with dashed lines.

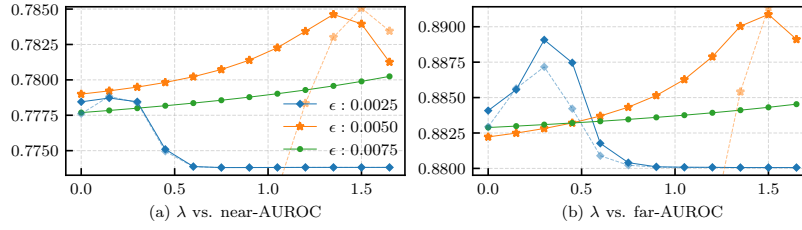


Fig. 4: Results by varying ϵ and λ on ImageNet-1K ID. Solid lines: A validation set is used to find the optimal J with $J_{\text{scaling}} = 2.0$. Dashed lines: No validation set calibration for J (results for $\epsilon = 0.0075$ falls out of the range of the plot).

6 Conclusion

In this study, we present TULiP, an uncertainty estimator for OOD detection. Our method is driven by the fluctuations under linearized training dynamics and excels in practical experiments. However, there are some limitations and future works remaining. Theoretically, our framework only considers functional perturbation. The perturbation on the NTK is also important [29] and could be integrated into the estimator in the future. Future works may improve upon these aspects, covering a wider range of OOD data by examining the network parameters and refining weight perturbations. In a broader aspect, exploring TULiP in other learning paradigms, such as Active Learning [51] or Reinforcement Learning [47] will be valuable.

Acknowledgments. This work was partially supported by JSPS KAKENHI Grant Numbers 20H00576, 23H03460, and 24K14849.

Disclosure of Interests. The authors have no competing interests to declare that are relevant to the content of this article.

References

1. Atakishiyev, S., Salameh, M., Yao, H., Goebel, R.: Explainable artificial intelligence for autonomous driving: A comprehensive overview and field guide for future research directions. *IEEE Access* **12**, 101603–101625 (2024)
2. Avron, H., Toledo, S.: Randomized algorithms for estimating the trace of an implicit symmetric positive semi-definite matrix. *Journal of the ACM* **58**(2), 1–34 (2011)
3. Baek, E., Park, K., Kim, J., Kim, H.S.: Unexplored faces of robustness and out-of-distribution: Covariate shifts in environment and sensor domains. In: *Proceedings of the IEEE/CVF CVPR*. pp. 22294–22303 (2024)
4. Bitterwolf, J., Müller, M., Hein, M.: In or out? fixing imagenet out-of-distribution detection evaluation (2023)
5. Blundell, C., Cornebise, J., Kavukcuoglu, K., Wierstra, D.: Weight uncertainty in neural network. In: *ICML*. vol. 37, pp. 1613–1622 (2015)

6. Chen, Z., Rotskoff, G., Bruna, J., Vanden-Eijnden, E.: A dynamical central limit theorem for shallow neural networks. In: *NeurIPS*. vol. 33, pp. 22217–22230 (2020)
7. Cimpoi, M., Maji, S., Kokkinos, I., Mohamed, S., Vedaldi, A.: Describing textures in the wild. In: *2014 IEEE CVPR*. pp. 3606–3613 (2014)
8. Daxberger, E., Kristiadi, A., Immer, A., Eschenhagen, R., Bauer, M., Hennig, P.: Laplace redux - effortless bayesian deep learning. In: *NeurIPS*. vol. 34, pp. 20089–20103 (2021)
9. Deng, J., Dong, W., Socher, R., Li, L.J., Li, K., Fei-Fei, L.: Imagenet: A large-scale hierarchical image database. In: *2009 IEEE CVPR*. pp. 248–255 (2009)
10. DeVries, T., Taylor, G.W.: Learning confidence for out-of-distribution detection in neural networks. *arXiv preprint arXiv:1802.04865* (2018)
11. Djuricic, A., Bozanic, N., Ashok, A., Liu, R.: Extremely simple activation shaping for out-of-distribution detection. In: *ICLR* (2023)
12. Du, S., Lee, J., Li, H., Wang, L., Zhai, X.: Gradient descent finds global minima of deep neural networks. In: *ICML*. vol. 97, pp. 1675–1685 (2019)
13. Esteva, A., Kuprel, B., Novoa, R.A., Ko, J., Swetter, S.M., Blau, H.M., Thrun, S.: Dermatologist-level classification of skin cancer with deep neural networks. *Nature* **542**(7639), 115–118 (2017)
14. Fort, S., Dziugaite, G.K., Paul, M., Kharaghani, S., Roy, D.M., Ganguli, S.: Deep learning versus kernel learning: an empirical study of loss landscape geometry and the time evolution of the neural tangent kernel. In: *NeurIPS*. vol. 33, pp. 5850–5861 (2020)
15. Gal, Y., Ghahramani, Z.: Dropout as a bayesian approximation: Representing model uncertainty in deep learning. In: *ICML*. vol. 48, pp. 1050–1059 (2016)
16. Geiger, M., Spigler, S., Jacot, A., Wyart, M.: Disentangling feature and lazy training in deep neural networks. *Journal of Statistical Mechanics: Theory and Experiment* **2020**(11), 113301 (2020)
17. Guo, C., Pleiss, G., Sun, Y., Weinberger, K.Q.: On calibration of modern neural networks. In: *ICML*. vol. 70, pp. 1321–1330 (2017)
18. He, B., Lakshminarayanan, B., Teh, Y.W.: Bayesian deep ensembles via the neural tangent kernel. In: *NeurIPS*. vol. 33, pp. 1010–1022 (2020)
19. He, K., Zhang, X., Ren, S., Sun, J.: Deep residual learning for image recognition. In: *2016 IEEE CVPR*. pp. 770–778 (2016)
20. Hendrycks, D., Basart, S., Mazeika, M., Zou, A., Kwon, J., Mostajabi, M., Steinhardt, J., Song, D.: Scaling out-of-distribution detection for real-world settings. In: *ICML*. vol. 162, pp. 8759–8773 (2022)
21. Hendrycks, D., Basart, S., Mu, N., Kadavath, S., Wang, F., Dorundo, E., Desai, R., Zhu, T., Parajuli, S., Guo, M., Song, D., Steinhardt, J., Gilmer, J.: The many faces of robustness: A critical analysis of out-of-distribution generalization. In: *Proceedings of the IEEE/CVF ICCV*. pp. 8340–8349 (2021)
22. Hendrycks, D., Dietterich, T.: Benchmarking neural network robustness to common corruptions and perturbations. In: *ICLR* (2019)
23. Hendrycks, D., Gimpel, K.: A baseline for detecting misclassified and out-of-distribution examples in neural networks. In: *ICLR* (2017)
24. Hora, S.C.: Aleatory and epistemic uncertainty in probability elicitation with an example from hazardous waste management. *Reliability Engineering & System Safety* **54**(2), 217–223 (1996)
25. Huang, R., Geng, A., Li, Y.: On the importance of gradients for detecting distributional shifts in the wild. In: *NeurIPS*. vol. 34, pp. 677–689 (2021)
26. Huang, R., Li, Y.: Mos: Towards scaling out-of-distribution detection for large semantic space. In: *Proceedings of the IEEE/CVF CVPR*. pp. 8710–8719 (2021)

27. Ioffe, S., Szegedy, C.: Batch normalization: accelerating deep network training by reducing internal covariate shift. In: ICML. vol. 37, p. 448–456 (2015)
28. Jacot, A., Gabriel, F., Hongler, C.: Neural tangent kernel: Convergence and generalization in neural networks. In: NeurIPS. vol. 31 (2018)
29. Kobayashi, S., Vilimelis Aceituno, P., von Oswald, J.: Disentangling the predictive variance of deep ensembles through the neural tangent kernel. In: NeurIPS. vol. 35, pp. 25335–25348 (2022)
30. Krizhevsky, A.: Learning multiple layers of features from tiny images. Master’s thesis, University of Tront (2009)
31. Kuznetsova, A., Rom, H., Alldrin, N., Uijlings, J., Krasin, I., Pont-Tuset, J., Kamali, S., Popov, S., Mallocci, M., Kolesnikov, A., et al.: The open images dataset v4: Unified image classification, object detection, and visual relationship detection at scale. *International Journal of Computer Vision* **128**(7), 1956–1981 (2020)
32. Lakshminarayanan, B., Pritzel, A., Blundell, C.: Simple and scalable predictive uncertainty estimation using deep ensembles. In: NeurIPS. vol. 30 (2017)
33. Le, Y., Yang, X.: Tiny imagenet visual recognition challenge. Class CS 231N, Stanford University (2015)
34. Lecun, Y., Bottou, L., Bengio, Y., Haffner, P.: Gradient-based learning applied to document recognition. *Proceedings of the IEEE* **86**(11), 2278–2324 (1998)
35. Lee, J., Sohl-dickstein, J., Pennington, J., Novak, R., Schoenholz, S., Bahri, Y.: Deep neural networks as gaussian processes. In: ICLR (2018)
36. Lee, J., Xiao, L., Schoenholz, S., Bahri, Y., Novak, R., Sohl-Dickstein, J., Pennington, J.: Wide neural networks of any depth evolve as linear models under gradient descent. In: NeurIPS. vol. 32 (2019)
37. Lee, K., Lee, K., Lee, H., Shin, J.: A simple unified framework for detecting out-of-distribution samples and adversarial attacks. In: NeurIPS. vol. 31 (2018)
38. Liang, S., Li, Y., Srikant, R.: Enhancing the reliability of out-of-distribution image detection in neural networks. In: ICLR (2018)
39. Liu, W., Wang, X., Owens, J., Li, Y.: Energy-based out-of-distribution detection. In: NeurIPS. vol. 33, pp. 21464–21475 (2020)
40. Liu, X., Lochman, Y., Zach, C.: Gen: Pushing the limits of softmax-based out-of-distribution detection. In: 2023 IEEE/CVF CVPR. pp. 23946–23955 (2023)
41. Netzer, Y., Wang, T., Coates, A., Bissacco, A., Wu, B., Ng, A.Y.: Reading digits in natural images with unsupervised feature learning. In: NeurIPS Workshop on Deep Learning and Unsupervised Feature Learning (2011)
42. Novak, R., Xiao, L., Hron, J., Lee, J., Alemi, A.A., Sohl-Dickstein, J., Schoenholz, S.S.: Neural tangents: Fast and easy infinite neural networks in python. In: ICLR (2020)
43. Russakovsky, O., Deng, J., Su, H., Krause, J., Satheesh, S., Ma, S., Huang, Z., Karpathy, A., Khosla, A., Bernstein, M., Berg, A.C., Fei-Fei, L.: Imagenet large scale visual recognition challenge. *International Journal of Computer Vision* **115**(3), 211–252 (2015)
44. Song, Y., Sebe, N., Wang, W.: Rankfeat: Rank-1 feature removal for out-of-distribution detection. In: NeurIPS. vol. 35, pp. 17885–17898 (2022)
45. Sun, Y., Guo, C., Li, Y.: React: Out-of-distribution detection with rectified activations. In: NeurIPS. vol. 34, pp. 144–157 (2021)
46. Sun, Y., Guo, C., Li, Y.: React: Out-of-distribution detection with rectified activations. *CoRR* **abs/2111.12797** (2021)
47. Szepesvari, C.: Algorithms for Reinforcement Learning (2010)

48. Van Horn, G., Mac Aodha, O., Song, Y., Cui, Y., Sun, C., Shepard, A., Adam, H., Perona, P., Belongie, S.: The inaturalist species classification and detection dataset. In: 2018 IEEE/CVF CVPR. pp. 8769–8778 (2018)
49. Vaze, S., Han, K., Vedaldi, A., Zisserman, A.: Open-set recognition: A good closed-set classifier is all you need. In: ICLR (2022)
50. Wang, H., Yeung, D.Y.: A survey on bayesian deep learning. ACM Comput. Surv. **53**(5) (2020)
51. Wang, H., Huang, W., Wu, Z., Tong, H., Margenot, A.J., He, J.: Deep active learning by leveraging training dynamics. In: NeurIPS. vol. 35, pp. 25171–25184 (2022)
52. Wang, H., Li, Z., Feng, L., Zhang, W.: Vim: Out-of-distribution with virtual-logit matching. In: Proceedings of the IEEE/CVF CVPR. pp. 4921–4930 (2022)
53. Yang, J., Wang, P., Zou, D., Zhou, Z., Ding, K., PENG, W., Wang, H., Chen, G., Li, B., Sun, Y., Du, X., Zhou, K., Zhang, W., Hendrycks, D., Li, Y., Liu, Z.: OpenOOD: Benchmarking generalized out-of-distribution detection. In: NeurIPS Datasets and Benchmarks Track (2022)
54. Yang, J., Zhou, K., Li, Y., Liu, Z.: Generalized out-of-distribution detection: A survey. International Journal of Computer Vision (2024)
55. Zhang, C., Bengio, S., Hardt, M., Recht, B., Vinyals, O.: Understanding deep learning requires rethinking generalization. In: ICLR (2017)
56. Zhang, J., Yang, J., Wang, P., Wang, H., Lin, Y., Zhang, H., Sun, Y., Du, X., Zhou, K., Zhang, W., Li, Y., Liu, Z., Chen, Y., Li, H.: Openood v1.5: Enhanced benchmark for out-of-distribution detection (2023)
57. Zhou, B., Lapedriza, A., Khosla, A., Oliva, A., Torralba, A.: Places: A 10 million image database for scene recognition. IEEE Transactions on Pattern Analysis and Machine Intelligence **40**(6), 1452–1464 (2018)

A Proofs

A.1 Basic notations

For a network $f(\mathbf{x}) : \mathbb{R}^d \rightarrow \mathbb{R}^o$ maps inputs \mathbf{x} of dimension d to outputs $f(\mathbf{x})$ of dimension o , parameterized by $\boldsymbol{\theta}$ with $|\boldsymbol{\theta}|$ trainable parameters, the gradient / Jacobian matrix $\nabla_{\boldsymbol{\theta}} f(\mathbf{x})$ is a $o \times |\boldsymbol{\theta}|$ matrix.

The NTK $\Theta(\mathbf{z}, \mathbf{x}) := \nabla_{\boldsymbol{\theta}} f(\mathbf{z}) \nabla_{\boldsymbol{\theta}} f(\mathbf{x})^\top$ is a $o \times o$ matrix.

$\ell'(f_t(\mathbf{x}))$ is the gradient of loss function w.r.t. network output $f_t(\mathbf{x})$ at training time t . It is, for convenience, a $o \times 1$ column-vector.

The following lemma will be useful thereafter, which is an application of Hölder’s inequality.

Lemma 1. *Let $F : \mathbf{x} \rightarrow \mathbb{R}^{m \times n}$, $g : \mathbf{x} \rightarrow \mathbb{R}^n$. Consider 2-norms $\|\cdot\|$ (i.e., euclidean and its induced matrix 2-norm). For $p, q \in [1, \infty]$ that $\frac{1}{p} + \frac{1}{q} = 1$, we have*

$$\begin{aligned}
& \|\mathbb{E}_{\mathbf{x}}[F(\mathbf{x})g(\mathbf{x})]\| \\
& \leq \mathbb{E}_{\mathbf{x}}[\|F(\mathbf{x})g(\mathbf{x})\|] \\
& \leq \mathbb{E}_{\mathbf{x}}[\|F(\mathbf{x})\| \cdot \|g(\mathbf{x})\|] \\
& \leq \mathbb{E}_{\mathbf{x}}[\|F(\mathbf{x})\|^p]^{1/p} \cdot \mathbb{E}_{\mathbf{x}}[\|g(\mathbf{x})\|^q]^{1/q}.
\end{aligned}$$

When $q = \infty$, we have $\mathbb{E}_{\mathbf{x}} [\|g(\mathbf{x})\|^q]^{1/q} := \sup_{\mathbf{x}} \|g(\mathbf{x})\|$.

For convenience, given any random variable, vector or matrix \mathbf{A} dependent of \mathbf{x} , we denote:

$$\|\mathbf{A}\|_X^{(q)} := \mathbb{E}_{\mathbf{x}} [\|\mathbf{A}\|^q]^{1/q}, \quad (12)$$

which by itself is a valid norm. We omit superscript (q) if $q = 2$.

A.2 Assumptions

We recall the assumptions here, which are originally shown in Sec. 3. For network $f(\mathbf{x}, \boldsymbol{\theta})$, dataset X with no parallel datapoints and a twice-differentiable loss function ℓ , we assume the followings:

- A1. (Boundedness) For $t \in [0, T]$, $f(\mathbf{x})$, $\nabla_{\boldsymbol{\theta}} f(\mathbf{x})$, ℓ and ℓ' stay bounded, uniformly on \mathbf{x} .
- A2. (Smoothness) Gradient ℓ' of loss function ℓ is Lipschitz continuous: $\forall x \in X$; $\|\ell'(\hat{y}; y(\mathbf{x})) - \ell'(\hat{y}'; y(\mathbf{x}))\| \leq L\|\hat{y} - \hat{y}'\|$.
- A3. (Perturbation) The perturbation Δf can be uniformly bounded by a constant α , that is, for all \mathbf{x} (not limited to the support of training data), i.e., $\forall x \in \mathbb{R}^d$; $\|\Delta f(\mathbf{x})\| \leq \alpha$.
- A4. (Convergence) Finally, for the original network trained via equation 3 and the perturbed network trained via equation 4, we assume *near-perfect convergence* on the training set \mathbf{x} at termination time $t = T$, i.e., $\exists \beta \in \mathbb{R}, \forall x \in X$; $\|f_T(\mathbf{x}) - \hat{f}_T(\mathbf{x})\| \leq \beta$.

A.3 Proof of Equation 5

We proof Thm. 1 (equation 5 and equation 6) separately.

Theorem 2. (Equation 5) Under assumptions A1-A4, for a network f trained with equation 3 and a perturbed network \hat{f} trained with equation 4, the perturbation applied at time $t_s = T - \Delta T$ bounded by α , we have

$$\|f_T(\mathbf{z}) - \hat{f}_T(\mathbf{z})\| \leq \inf_{\mathbf{x} \in X} C \|\nabla_{\boldsymbol{\theta}} f(\mathbf{z}) - \nabla_{\boldsymbol{\theta}} f(\mathbf{x})\|_F + 2\alpha + \beta, \quad (13)$$

where $C = \frac{\alpha \eta \bar{\Theta}_X^{1/2}}{\lambda_{max}} (e^{(T-t_s)L\lambda_{max}} - 1)$, $\bar{\Theta}_X^{1/2} := \|\nabla_{\boldsymbol{\theta}} f(\mathbf{x})\|_X$ is the average gradient norm over training data, and $\lambda_{max} := \frac{1}{\sqrt{N}} \|\mathbf{G}\|$ for a generalized Gram matrix $G_{i,j} := \|\Theta(x_i, x_j)\|$ of dataset $X = \{x_1, x_2, \dots, x_N\}$.

Proof. Let us first examine the fluctuations in the training set. From the Lipschitz continuity of ℓ' ,

$$\left\| \ell'(f_t(\mathbf{x})) - \ell'(\hat{f}_t(\mathbf{x})) \right\|_X \leq L \|f(\mathbf{x}) - \hat{f}(\mathbf{x})\|_X. \quad (14)$$

Thus, by the linearized dynamics we have

$$\begin{aligned}
& \partial_t \left\| f_t(\mathbf{x}) - \hat{f}_t(\mathbf{x}) \right\|_X \\
& \leq \left\| \partial_t \left(f_t(\mathbf{x}) - \hat{f}_t(\mathbf{x}) \right) \right\|_X \\
& = \left\| \mathbb{E}_{\mathbf{x}'} \left[\Theta(\mathbf{x}, \mathbf{x}') \left(\ell'(f_t(\mathbf{x}')) - \ell'(\hat{f}_t(\mathbf{x}')) \right) \right] \right\|_X
\end{aligned} \tag{15}$$

$$\begin{aligned}
& = \mathbb{E}_{\mathbf{x}} \left[\left\| \mathbb{E}_{\mathbf{x}'} \left[\Theta(\mathbf{x}, \mathbf{x}') \left(\ell'(f_t(\mathbf{x}')) - \ell'(\hat{f}_t(\mathbf{x}')) \right) \right] \right\|^2 \right]^{1/2} \\
& \leq \mathbb{E}_{\mathbf{x}} \left[\left\| \Theta(\mathbf{x}, \mathbf{x}') \right\|_X^2 \left\| \ell'(f_t(\mathbf{x}')) - \ell'(\hat{f}_t(\mathbf{x}')) \right\|_X^2 \right]^{1/2} \\
& \leq \mathbb{E}_{\mathbf{x}, \mathbf{x}'} \left[\left\| \Theta(\mathbf{x}, \mathbf{x}') \right\|^2 \right]^{1/2} \left\| \ell'(f_t(\mathbf{x})) - \ell'(\hat{f}_t(\mathbf{x})) \right\|_X \\
& \leq L\lambda_{max} \left\| f_t(\mathbf{x}) - \hat{f}_t(\mathbf{x}) \right\|_X,
\end{aligned} \tag{16}$$

where in equation 15 we have used the triangle inequality to put ∂_t inside the norm. λ_{max} is defined as $\frac{1}{\sqrt{N}} \|\mathbf{G}\|$ for a generalized Gram-matrix $\mathbf{G}_{ij} := \|\Theta(x_i, x_j)\|$ of dataset $X = \{x_1, x_2, \dots, x_N\}$, measures the fitness (or alignment) of the kernel Θ w.r.t. the training data.

From equation 16, we can apply the Grönwall's inequality to obtain

$$\begin{aligned}
& \left\| f_t(\mathbf{x}) - \hat{f}_t(\mathbf{x}) \right\|_X \\
& \leq \left\| f_{t_s}(\mathbf{x}) - \hat{f}_{t_s}(\mathbf{x}) \right\|_X e^{(t-t_s)L\lambda_{max}} \\
& \leq \alpha e^{(t-t_s)L\lambda_{max}}.
\end{aligned} \tag{17}$$

We now prove Theorem 3.1 by generalizing equation 17 to given test data.

For a test point $z \in \mathbb{R}^d$, choose a pivot point $\mathbf{x}^* \in X$ from the training set. Then for the network function f evaluated at \mathbf{x}^* and z , we have the followings:

$$\begin{aligned}
& \left| \partial_t \left\| (f_t(z) - f_t(\mathbf{x}^*)) - (\hat{f}_t(z) - \hat{f}_t(\mathbf{x}^*)) \right\| \right| \\
& \leq \left\| \partial_t \left[(f_t(z) - f_t(\mathbf{x}^*)) - (\hat{f}_t(z) - \hat{f}_t(\mathbf{x}^*)) \right] \right\| \\
& = \eta \left\| \mathbb{E}_{\mathbf{x}} \left[(\Theta(z, \mathbf{x}) - \Theta(\mathbf{x}^*, \mathbf{x})) \cdot (\ell'(f_t(\mathbf{x})) - \ell'(\hat{f}_t(\mathbf{x}))) \right] \right\|
\end{aligned} \tag{18}$$

Denote

$$\left\| (f_t(z) - f_t(\mathbf{x}^*)) - (\hat{f}_t(z) - \hat{f}_t(\mathbf{x}^*)) \right\|$$

as $\Delta f_t(\mathbf{z})$, and let $\Theta_{\mathbf{x}^*}^{\text{diff}}(\mathbf{z}, \mathbf{x}) := (\Theta(\mathbf{z}, \mathbf{x}) - \Theta(\mathbf{x}^*, \mathbf{x}))$. Integrate equation 18 with t , we have

$$\begin{aligned}
& |\Delta f_T(\mathbf{z}) - \Delta f_{t_s}(\mathbf{z})| \\
& \leq \eta \int_{t_s}^T \left\| \mathbb{E}_{\mathbf{x}} \left[\Theta_{\mathbf{x}^*}^{\text{diff}}(\mathbf{z}, \mathbf{x}) \left(\ell'(f_t(\mathbf{x})) - \ell'(\hat{f}_t(\mathbf{x})) \right) \right] \right\| dt \\
& \leq \eta \int_{t_s}^T \left\| \Theta_{\mathbf{x}^*}^{\text{diff}}(\mathbf{z}, \mathbf{x}) \right\|_X \left\| \ell'(f_t(\mathbf{x})) - \ell'(\hat{f}_t(\mathbf{x})) \right\|_X dt \\
& \leq \eta L \left\| \Theta_{\mathbf{x}^*}^{\text{diff}}(\mathbf{z}, \mathbf{x}) \right\|_X \int_{t_s}^T \left\| f_t(\mathbf{x}) - \hat{f}_t(\mathbf{x}) \right\|_X dt
\end{aligned} \tag{19}$$

We start with the term before the integral. To begin, rewrite it as:

$$\begin{aligned}
& \left\| \Theta(\mathbf{z}, \mathbf{x}) - \Theta(\mathbf{x}^*, \mathbf{x}) \right\|_X \\
& = \left\| (\nabla_{\boldsymbol{\theta}} f(\mathbf{z}) - \nabla_{\boldsymbol{\theta}} f(\mathbf{x}^*)) \nabla_{\boldsymbol{\theta}} f(\mathbf{x})^\top \right\|_X \\
& \leq \mathbb{E}_{\mathbf{x}} \left[\left\| \nabla_{\boldsymbol{\theta}} f(\mathbf{z}) - \nabla_{\boldsymbol{\theta}} f(\mathbf{x}^*) \right\|^2 \cdot \left\| \nabla_{\boldsymbol{\theta}} f(\mathbf{x}) \right\|^2 \right]^{1/2} \\
& = \left\| \nabla_{\boldsymbol{\theta}} f(\mathbf{z}) - \nabla_{\boldsymbol{\theta}} f(\mathbf{x}^*) \right\| \cdot \left\| \nabla_{\boldsymbol{\theta}} f(\mathbf{x}) \right\|_X \\
& \leq \left\| \nabla_{\boldsymbol{\theta}} f(\mathbf{z}) - \nabla_{\boldsymbol{\theta}} f(\mathbf{x}^*) \right\|_{\text{F}} \cdot \bar{\Theta}_X^{1/2},
\end{aligned} \tag{20}$$

where $\bar{\Theta}_X^{1/2} := \left\| \nabla_{\boldsymbol{\theta}} f(\mathbf{x}) \right\|_X$ is independent from \mathbf{z} .

Remark 1. equation 20 used a computationally friendly Frobenius norm to bound the spectral norm in the line right above it. This is the main motivation to use a \sqrt{o} scaling for hyper-parameter λ , as $\|\mathbf{A}\|_2 \leq \|\mathbf{A}\|_F \leq \sqrt{o} \|\mathbf{A}\|_2$ given \mathbf{A} is full-rank $o \times |\boldsymbol{\theta}|$ and $o < |\boldsymbol{\theta}|$.

Bring equation 20 and equation 17 back to equation 19 we have

$$\begin{aligned}
& |\Delta f_T(\mathbf{z}) - \Delta f_{t_s}(\mathbf{z})| \\
& \leq \left\| \nabla_{\boldsymbol{\theta}} f(\mathbf{z}) - \nabla_{\boldsymbol{\theta}} f(\mathbf{x}^*) \right\|_{\text{F}} \frac{\alpha \eta \bar{\Theta}_X^{1/2}}{\lambda_{\max}} \left(e^{(T-t_s)L\lambda_{\max}} - 1 \right).
\end{aligned} \tag{21}$$

Finally, we bound the difference between $f_T(\mathbf{z})$ and $\hat{f}_T(\mathbf{z})$ via the triangle inequality.

First, observe that from A3,

$$\begin{aligned}
\Delta f_{t_s}(\mathbf{z}) & = \left\| (f_{t_s}(\mathbf{z}) - f_{t_s}(\mathbf{x}^*)) - (\hat{f}_{t_s}(\mathbf{z}) - \hat{f}_{t_s}(\mathbf{x}^*)) \right\| \\
& \leq \left\| f_{t_s}(\mathbf{z}) - \hat{f}_{t_s}(\mathbf{z}) \right\| + \left\| \hat{f}_{t_s}(\mathbf{x}^*) - f_{t_s}(\mathbf{x}^*) \right\| \\
& \leq 2\alpha,
\end{aligned} \tag{22}$$

so that

$$\begin{aligned}
\Delta f_T(\mathbf{z}) & \leq |\Delta f_T(\mathbf{z}) - \Delta f_{t_s}(\mathbf{z})| + |\Delta f_{t_s}(\mathbf{z})| \\
& \leq \left\| \nabla_{\boldsymbol{\theta}} f(\mathbf{z}) - \nabla_{\boldsymbol{\theta}} f(\mathbf{x}^*) \right\|_{\text{F}} \frac{\alpha \eta \bar{\Theta}_X^{1/2}}{\lambda_{\max}} \left(e^{(T-t_s)L\lambda_{\max}} - 1 \right) + 2\alpha.
\end{aligned} \tag{23}$$

Thus, given the convergence assumption $\|f_T(\mathbf{x}^*) - \hat{f}_T(\mathbf{x}^*)\| \leq \beta$ (A4),

$$\begin{aligned} & \left\| f_T(\mathbf{z}) - \hat{f}_T(\mathbf{z}) \right\| \\ &= \left\| \left(f_T(\mathbf{z}) - f_T(\mathbf{x}^*) \right) - \left(\hat{f}_T(\mathbf{z}) - \hat{f}_T(\mathbf{x}^*) \right) - \left(\hat{f}_T(\mathbf{x}^*) - f_T(\mathbf{x}^*) \right) \right\| \\ &\leq \Delta f_T(\mathbf{z}) + \beta. \end{aligned} \quad (24)$$

To proceed, recall that \mathbf{x}^* is chosen arbitrarily. This concludes the proof.

We can further write the equation as:

$$\inf_{\mathbf{x} \in X} \|\nabla_{\boldsymbol{\theta}} f(\mathbf{z}) - \nabla_{\boldsymbol{\theta}} f(\mathbf{x})\|_F = \inf_{\mathbf{x} \in X} [\text{Tr}(\Theta(\mathbf{z}, \mathbf{z}) + \Theta(\mathbf{x}, \mathbf{x}) - 2\Theta(\mathbf{z}, \mathbf{x}))]^{1/2}. \quad (25)$$

Note for equation 25: Let $\mathbf{A} := \nabla_{\boldsymbol{\theta}} f(\mathbf{z}) - \nabla_{\boldsymbol{\theta}} f(\mathbf{x})$. Then, we have $\text{Tr}(\mathbf{A}\mathbf{A}^\top) = \text{Tr}(\Theta(\mathbf{z}, \mathbf{z}) + \Theta(\mathbf{x}, \mathbf{x}) - \Theta(\mathbf{z}, \mathbf{x}) - \Theta(\mathbf{x}, \mathbf{z}))$. Note that $\Theta(\mathbf{x}, \mathbf{z}) = \Theta(\mathbf{z}, \mathbf{x})^\top$ and therefore we may substitute them inside the trace. Thereafter, using $\|\mathbf{A}\|_F = (\text{Tr}(\mathbf{A}\mathbf{A}^\top))^{1/2}$, we can obtain equation 25.

A.4 Proof of Equation 6

We first present the following lemma under the weakly lazy regime, i.e., we allow the weak dependency of Θ_t on t . Let us define $|\Theta_T(\mathbf{z}, \mathbf{x})|$ as the unique symmetric positive semi-definite solution of $|\Theta_T(\mathbf{z}, \mathbf{x})|^2 = \Theta_T(\mathbf{z}, \mathbf{x})^\top \Theta_T(\mathbf{z}, \mathbf{x})$, which is an extension of absolute values to matrices.

Lemma 2. *We assume the lazy learning regime, i.e., there exists $\delta > 0$ such that $\sup_{\mathbf{x}, \mathbf{x}'} \||\Theta_T(\mathbf{x}, \mathbf{x}')| - |\Theta_t(\mathbf{x}, \mathbf{x}')|\| \leq \delta$ holds for all $t_s \leq t \leq T$. Under assumption A1, with the model parameters $\boldsymbol{\theta}_T$ trained from $\boldsymbol{\theta}_{t_s}$ with equation 3 over the training set \mathbf{x} and $t_s < T$, we have:*

$$\|\nabla_{\boldsymbol{\theta}} f_T(\mathbf{z})(\boldsymbol{\theta}_T - \boldsymbol{\theta}_{t_s})\| \leq C(\text{Tr}\mathbb{E}_{\mathbf{x}}[|\Theta_T(\mathbf{z}, \mathbf{x})|] + o\delta) + \sqrt{\delta}\|\boldsymbol{\theta}_T - \boldsymbol{\theta}_{t_s}\| \quad (26)$$

where C is a positive constant independent of \mathbf{z} .

Proof. The mean value theorem for integrals guarantees that there exists $\tau \in [t_s, T]$ such that

$$\boldsymbol{\theta}_T - \boldsymbol{\theta}_{t_s} = - \int_{t_s}^T \eta \mathbb{E}_{\mathbf{x}} [\nabla_{\boldsymbol{\theta}} f_\tau(\mathbf{x}) \ell'(f_\tau(\mathbf{x}))] dt. \quad (27)$$

Then, Hölder's inequality leads to

$$\begin{aligned} \|\nabla_{\boldsymbol{\theta}} f_\tau(\mathbf{z})(\boldsymbol{\theta}_T - \boldsymbol{\theta}_{t_s})\| &= \left\| \mathbb{E}_{\mathbf{x}} \left[\nabla_{\boldsymbol{\theta}} f_\tau(\mathbf{z}) \nabla_{\boldsymbol{\theta}} f_\tau(\mathbf{x})^\top \eta \int_{t_s}^T \ell'(f_\tau(\mathbf{x})) dt \right] \right\| \\ &\leq \|\Theta_\tau(\mathbf{z}, \mathbf{x})\|_X^{(1)} \cdot \underbrace{\left\| \eta \int_{t_s}^T \ell'(f_\tau(\mathbf{x})) dt \right\|_X^{(\infty)}}_{\text{independent of } \mathbf{z}}. \end{aligned} \quad (28)$$

The lazy learning assumption leads that

$$\begin{aligned}
\|\Theta_\tau(\mathbf{z}, \mathbf{x})\|_X^{(1)} &\leq \mathbb{E}_{\mathbf{x}} \left[\text{Tr} (\Theta_\tau(\mathbf{z}, \mathbf{x})^\top \Theta_\tau(\mathbf{z}, \mathbf{x}))^{1/2} \right] \\
&\leq \mathbb{E}_{\mathbf{x}} [\text{Tr} (|\Theta_\tau(\mathbf{z}, \mathbf{x})|)] \\
&\leq \mathbb{E}_{\mathbf{x}} [\text{Tr} (|\Theta_T(\mathbf{z}, \mathbf{x})|)] + o\delta \\
&= \text{Tr} (\mathbb{E}_{\mathbf{x}} [|\Theta_T(\mathbf{z}, \mathbf{x})|]) + o\delta.
\end{aligned}$$

Again the lazy learning assumption for $|\Theta_T(\mathbf{z}, \mathbf{z})| = \Theta_T(\mathbf{z}, \mathbf{z})$ ensures that

$$\begin{aligned}
\|\nabla_{\boldsymbol{\theta}} f_\tau(\mathbf{z})(\boldsymbol{\theta}_T - \boldsymbol{\theta}_{t_s})\|^2 &= (\boldsymbol{\theta}_T - \boldsymbol{\theta}_{t_s})^T \Theta_\tau(\mathbf{z}, \mathbf{z})(\boldsymbol{\theta}_T - \boldsymbol{\theta}_{t_s}) \\
&\geq (\boldsymbol{\theta}_T - \boldsymbol{\theta}_{t_s})^T (\Theta_T(\mathbf{z}, \mathbf{z}) - \delta \mathbf{I})(\boldsymbol{\theta}_T - \boldsymbol{\theta}_{t_s}) \\
&= \|\nabla_{\boldsymbol{\theta}} f_T(\mathbf{z})(\boldsymbol{\theta}_T - \boldsymbol{\theta}_{t_s})\|^2 - \delta \|\boldsymbol{\theta}_T - \boldsymbol{\theta}_{t_s}\|^2.
\end{aligned}$$

Hence, we have

$$\begin{aligned}
\|\nabla_{\boldsymbol{\theta}} f_\tau(\mathbf{z})(\boldsymbol{\theta}_T - \boldsymbol{\theta}_{t_s})\| &\leq \sqrt{\|\nabla_{\boldsymbol{\theta}} f_\tau(\mathbf{z})(\boldsymbol{\theta}_T - \boldsymbol{\theta}_{t_s})\|^2 + \delta \|\boldsymbol{\theta}_T - \boldsymbol{\theta}_{t_s}\|^2} \\
&\leq \|\nabla_{\boldsymbol{\theta}} f_\tau(\mathbf{z})(\boldsymbol{\theta}_T - \boldsymbol{\theta}_{t_s})\| + \sqrt{\delta} \|\boldsymbol{\theta}_T - \boldsymbol{\theta}_{t_s}\|.
\end{aligned}$$

Substituting the above inequalities into equation 28, we obtain the conclusion of the lemma.

By setting $\delta = 0$ in the above lemma, we are able to obtain equation 6 with A5 and equation 25.

A.5 Proof of Proposition 1

We proof the proposition with an optional, diagonal scaling matrix $\mathbf{\Gamma}$, i.e., by modifying equation 8 as:

$$\nabla_{\boldsymbol{\theta}} f_T^{emp}(\mathbf{z}) \mathbf{\Gamma}^2 \nabla_{\boldsymbol{\theta}} f_T^{emp}(\mathbf{x})^\top \approx \Theta(\mathbf{z}, \mathbf{x}). \quad (29)$$

Proposition 2. (Proposition 1 with scaling) Suppose that f^{emp} is γ -smooth w.r.t. $\boldsymbol{\theta}$, i.e.,

$$\|\nabla_{\boldsymbol{\theta}} f^{emp}(\mathbf{z}; \boldsymbol{\theta}) - \nabla_{\boldsymbol{\theta}} f^{emp}(\mathbf{z}; \boldsymbol{\theta}')\|_F \leq \gamma \|\boldsymbol{\theta} - \boldsymbol{\theta}'\|.$$

Let \mathbf{v} be a random variable such that $\mathbb{E}_{\mathbf{v}}[\mathbf{v}] = \mathbf{0}$, $\mathbb{E}_{\mathbf{v}}[\mathbf{v}\mathbf{v}^\top] = \epsilon^2 \mathbf{I}$ and $\mathbb{E}_{\mathbf{v}}[\|\mathbf{v}\|^k] \leq C_k \epsilon^k$ for $k = 3, 4$, where C_k is a constant depending on k and the dimension of \mathbf{v} . Then, under A1, it holds that

$$\lim_{\epsilon \rightarrow 0} \frac{1}{\epsilon^2} \mathbb{E}_{\mathbf{v}} [\|f^{emp}(\mathbf{z}; \boldsymbol{\theta}_T + \mathbf{\Gamma}\mathbf{v}) - f^{emp}(\mathbf{z}; \boldsymbol{\theta}_T)\|^2] = \text{Tr} (\nabla_{\boldsymbol{\theta}} f^{emp}(\mathbf{z}; \boldsymbol{\theta}_T) \mathbf{\Gamma}^2 \nabla_{\boldsymbol{\theta}} f^{emp}(\mathbf{z}; \boldsymbol{\theta}_T)^\top). \quad (30)$$

Proof. For each component $f_i^{emp}, i = 1, \dots, o$, the mean value theorem leads that there exists $t_i \in [0, 1]$ such that

$$\begin{aligned}
&|f_i^{emp}(\mathbf{z}; \boldsymbol{\theta}_T + \mathbf{\Gamma}\mathbf{v}) - f_i^{emp}(\mathbf{z}; \boldsymbol{\theta}_T) - \nabla_{\boldsymbol{\theta}} f_i^{emp}(\mathbf{z}; \boldsymbol{\theta}_T)^\top \mathbf{\Gamma}\mathbf{v}| \\
&= |\nabla_{\boldsymbol{\theta}} f_i^{emp}(\mathbf{z}; \boldsymbol{\theta}_T + t_i \mathbf{\Gamma}\mathbf{v})^\top \mathbf{\Gamma}\mathbf{v} - \nabla_{\boldsymbol{\theta}} f_i^{emp}(\mathbf{z}; \boldsymbol{\theta}_T)^\top \mathbf{\Gamma}\mathbf{v}| \\
&\leq \gamma \|\mathbf{\Gamma}\|^2 \|\mathbf{v}\|^2.
\end{aligned}$$

For real numbers $a_i, b_i, i = 1, \dots, o$, suppose $|a_i - b_i| \leq c$. Then, we have

$$\left| \sum_i a_i^2 - \sum_i b_i^2 \right| = \left| 2 \sum_i b_i(a_i - b_i) + \sum_i (a_i - b_i)^2 \right| \leq 2c \sum_i |b_i| + oc^2.$$

Using the above inequality, we obtain

$$\begin{aligned} & \left| \mathbb{E}_{\mathbf{v}} [\|f^{emp}(\mathbf{z}; \boldsymbol{\theta}_T + \boldsymbol{\Gamma}\mathbf{v}) - f^{emp}(\mathbf{z}; \boldsymbol{\theta}_T)\|^2] - \mathbb{E}_{\mathbf{v}} [\mathbf{v}^\top \boldsymbol{\Gamma} \nabla_{\boldsymbol{\theta}} f^{emp}(\mathbf{z}; \boldsymbol{\theta}_T)^\top \nabla_{\boldsymbol{\theta}} f^{emp}(\mathbf{z}; \boldsymbol{\theta}_T) \boldsymbol{\Gamma} \mathbf{v}] \right| \\ & \leq 2\gamma \|\boldsymbol{\Gamma}\|^2 \mathbb{E}_{\mathbf{v}} [\sum_i |\mathbf{v}^\top \boldsymbol{\Gamma} \nabla_{\boldsymbol{\theta}} f_i^{emp}(\mathbf{z}; \boldsymbol{\theta}_T)| \|\mathbf{v}\|^2] + o\gamma^2 \|\boldsymbol{\Gamma}\|^4 \mathbb{E}_{\mathbf{v}} [\|\mathbf{v}\|^4] \\ & \leq 2\sqrt{o}\gamma \|\boldsymbol{\Gamma}\|^3 \|\nabla_{\boldsymbol{\theta}} f^{emp}(\mathbf{z}; \boldsymbol{\theta}_T)\|_{\text{F}} \mathbb{E}_{\mathbf{v}} [\|\mathbf{v}\|^3] + o\gamma^2 \|\boldsymbol{\Gamma}\|^4 \mathbb{E}_{\mathbf{v}} [\|\mathbf{v}\|^4]. \end{aligned} \quad (31)$$

Note the cyclic trick for the trace ensures that

$$\begin{aligned} & \mathbb{E}_{\mathbf{v}} [\mathbf{v}^\top \boldsymbol{\Gamma} \nabla_{\boldsymbol{\theta}} f^{emp}(\mathbf{z}; \boldsymbol{\theta}_T)^\top \nabla_{\boldsymbol{\theta}} f^{emp}(\mathbf{z}; \boldsymbol{\theta}_T) \boldsymbol{\Gamma} \mathbf{v}] \\ & = \mathbb{E}_{\mathbf{v}} [\text{Tr} (\boldsymbol{\Gamma} \nabla_{\boldsymbol{\theta}} f^{emp}(\mathbf{z}; \boldsymbol{\theta}_T)^\top \nabla_{\boldsymbol{\theta}} f^{emp}(\mathbf{z}; \boldsymbol{\theta}_T) \boldsymbol{\Gamma} \mathbf{v} \mathbf{v}^\top)] \\ & = \text{Tr} (\boldsymbol{\Gamma} \nabla_{\boldsymbol{\theta}} f^{emp}(\mathbf{z}; \boldsymbol{\theta}_T)^\top \nabla_{\boldsymbol{\theta}} f^{emp}(\mathbf{z}; \boldsymbol{\theta}_T) \boldsymbol{\Gamma} \mathbb{E}_{\mathbf{v}} [\mathbf{v} \mathbf{v}^\top]) \\ & = \text{Tr} (\boldsymbol{\Gamma} \nabla_{\boldsymbol{\theta}} f^{emp}(\mathbf{z}; \boldsymbol{\theta}_T)^\top \nabla_{\boldsymbol{\theta}} f^{emp}(\mathbf{z}; \boldsymbol{\theta}_T) \boldsymbol{\Gamma} \cdot \epsilon^2 \mathbf{I}) \end{aligned} \quad (32)$$

$$= \epsilon^2 \text{Tr} (\nabla_{\boldsymbol{\theta}} f^{emp}(\mathbf{z}; \boldsymbol{\theta}_T) \boldsymbol{\Gamma}^2 \nabla_{\boldsymbol{\theta}} f^{emp}(\mathbf{z}; \boldsymbol{\theta}_T)^\top). \quad (33)$$

In equation 32 we applied the condition that $\mathbb{E}_{\mathbf{v}}[\mathbf{v} \mathbf{v}^\top] = \epsilon^2 \mathbf{I}$. We note that this is a slightly modified version of the well-known Hutchinson's Trace Estimator. We refer the readers to the existing analysis of such estimators [2] for more details. As a result, we obtain

$$\begin{aligned} & \left| \lim_{\epsilon \rightarrow 0} \frac{1}{\epsilon^2} \mathbb{E}_{\mathbf{v}} [\|f^{emp}(\mathbf{z}; \boldsymbol{\theta}_T + \boldsymbol{\Gamma}\mathbf{v}) - f^{emp}(\mathbf{z}; \boldsymbol{\theta}_T)\|^2] - \text{Tr} (\nabla_{\boldsymbol{\theta}} f^{emp}(\mathbf{z}; \boldsymbol{\theta}_T) \boldsymbol{\Gamma}^2 \nabla_{\boldsymbol{\theta}} f^{emp}(\mathbf{z}; \boldsymbol{\theta}_T)^\top) \right| \\ & \leq \lim_{\epsilon \rightarrow 0} 2\sqrt{o}\gamma \|\boldsymbol{\Gamma}\|^3 \|\nabla_{\boldsymbol{\theta}} f^{emp}(\mathbf{z}; \boldsymbol{\theta}_T)\|_{\text{F}} C_3 \epsilon + o\gamma^2 \|\boldsymbol{\Gamma}\|^4 C_4 \epsilon^2 \\ & = 0. \end{aligned}$$

The above equality means the conclusion of the proposition.

A.6 Additional derivations for Section 4.3

Under the distribution of \mathbf{v} we have

$$\begin{aligned} \mathbb{E}_{\mathbf{v}} [f^{emp}(\mathbf{z}; \boldsymbol{\theta}_T + \boldsymbol{\Gamma}\mathbf{v})] & = f^{emp}(\mathbf{z}; \boldsymbol{\theta}_T) + \underbrace{\mathbb{E}_{\mathbf{v}} [\nabla_{\boldsymbol{\theta}} f^{emp}(\mathbf{z}; \boldsymbol{\theta}_T)^\top \boldsymbol{\Gamma} \mathbf{v}]}_{=0 \text{ from } \mathbb{E}_{\mathbf{v}}[\mathbf{v}]=0} + O(\mathbb{E}[\mathbf{v}^2]) \\ & = f^{emp}(\mathbf{z}; \boldsymbol{\theta}_T) + O(\epsilon^2), \end{aligned}$$

which indicates that $\mathbb{E}_{\mathbf{v}} [f^{emp}(\mathbf{z}; \boldsymbol{\theta}_T + \boldsymbol{\Gamma}\mathbf{v})] \approx f^{emp}(\mathbf{z}; \boldsymbol{\theta}_T)$ when ϵ is small.

We continue by the computation of $\text{TrVar}[\tilde{f}^{\text{raw}}(\mathbf{z})]$:

$$\begin{aligned}\text{TrVar}_{\mathbf{v}}[\tilde{f}^{\text{raw}}(\mathbf{z})] &= \mathbb{E}_{\mathbf{v}}[\|f^{\text{emp}}(\mathbf{z}; \boldsymbol{\theta}_T + \Gamma \mathbf{v}) - \mathbb{E}_{\mathbf{v}}[f^{\text{emp}}(\mathbf{z}; \boldsymbol{\theta}_T + \Gamma \mathbf{v})]\|^2] \\ &= \mathbb{E}_{\mathbf{v}}[\|f^{\text{emp}}(\mathbf{z}; \boldsymbol{\theta}_T + \Gamma \mathbf{v}) - f^{\text{emp}}(\mathbf{z}; \boldsymbol{\theta}_T) + O(\epsilon^2)\|^2] \\ &= \mathbb{E}_{\mathbf{v}}[\|f^{\text{emp}}(\mathbf{z}; \boldsymbol{\theta}_T + \Gamma \mathbf{v}) - f^{\text{emp}}(\mathbf{z}; \boldsymbol{\theta}_T)\|^2] + O(\epsilon^4) \\ &\approx \epsilon^2 \text{Tr} \Theta(\mathbf{z}, \mathbf{z}) + O(\epsilon^4).\end{aligned}$$

Let $\tilde{\Theta}_{\text{Tr}}(\mathbf{z}, \mathbf{z})$ be an approximation of $\epsilon^2 \text{Tr} \Theta(\mathbf{z}, \mathbf{z})$, which is being computed empirically in line 11 of Alg. 1.

Thus, $\gamma^2 \text{TrVar}_{\mathbf{v}}[\tilde{f}^{\text{raw}}(\mathbf{z})]$ reads:

$$\begin{aligned}\gamma^2 \text{TrVar}_{\mathbf{v}}[\tilde{f}^{\text{raw}}(\mathbf{z})] &= \frac{[\tilde{\Theta}_{\text{Tr}}(\mathbf{z}, \mathbf{z}) - \lambda D]_+}{\tilde{\Theta}_{\text{Tr}}(\mathbf{z}, \mathbf{z})} \text{TrVar}_{\mathbf{v}}[\tilde{f}^{\text{raw}}(\mathbf{z})] \\ &\approx \frac{[\tilde{\Theta}_{\text{Tr}}(\mathbf{z}, \mathbf{z}) - \lambda D]_+}{\tilde{\Theta}_{\text{Tr}}(\mathbf{z}, \mathbf{z})} (\tilde{\Theta}_{\text{Tr}}(\mathbf{z}, \mathbf{z}) + O(\epsilon^4)) \\ &\approx [\epsilon^2 \text{Tr} \Theta(\mathbf{z}, \mathbf{z}) - \lambda D]_+ + O(\epsilon^4)\end{aligned}$$

where $[\cdot]_+$ denotes $\max(\cdot, 0)$.

For D , from approximation equation 9 we have

$$\begin{aligned}D &= \left\| f^{\text{emp}}(\mathbf{z}; \boldsymbol{\theta}_T + \epsilon \delta \Gamma(\boldsymbol{\theta}_T - \boldsymbol{\theta}_{t_s})) - f^{\text{emp}}(\mathbf{z}; \boldsymbol{\theta}_T) \right\| \\ &\approx \epsilon \delta \left\| \nabla_{\boldsymbol{\theta}} f_T(\mathbf{z})(\boldsymbol{\theta}_T - \boldsymbol{\theta}_{t_s}) \right\|.\end{aligned}$$

As a result, we have

$$\gamma^2 \text{TrVar}[\tilde{f}^{\text{raw}}(\mathbf{z})] \approx [\epsilon^2 \text{Tr} \Theta(\mathbf{z}, \mathbf{z}) - \epsilon \delta \left\| \nabla_{\boldsymbol{\theta}} f_T(\mathbf{z})(\boldsymbol{\theta}_T - \boldsymbol{\theta}_{t_s}) \right\|]_+.$$

Recall that equation 7 indicates that

$$\text{Tr}(\text{Var}_{\Delta f}[\hat{f}_T(\mathbf{z})]) \leq \mathbb{E}_{\Delta f}[\|\hat{f}_T(\mathbf{z}) - f_T(\mathbf{z})\|^2],$$

and Prop. 1 shows that

$$\|f_T(\mathbf{z}) - \hat{f}_T(\mathbf{z})\| \lesssim \left[\text{Tr}(\Theta(\mathbf{z}, \mathbf{z}) + \underbrace{\mathbb{E}_{\mathbf{x}}[\Theta(\mathbf{x}, \mathbf{x})]}_{\text{Independent of } \mathbf{z}}) - 2K \left\| \nabla_{\boldsymbol{\theta}} f_T(\mathbf{z})(\boldsymbol{\theta}_T - \boldsymbol{\theta}_{t_s}) \right\| \right]^{1/2}.$$

A.7 Perturb-then-train and equation 1

[28] consider neural networks in an infinite-width limit with specified initialization scheme, which we have referred as the lazy limit in Section 3. Under such limit, the linearized network equation 2 is justified as the empirical NTK (at initialization) converges to a specific deterministic kernel Θ , where the distribution of a neural network $f(\mathbf{x}; \boldsymbol{\theta})$'s initialization functional $f_{\text{Init}}(\mathbf{x})$ converges to a Gaussian Process (NNGP) [35]. In equation 2, it is equivalent to a deterministic (fixed) $\nabla_{\boldsymbol{\theta}} f_{\text{True}}(\mathbf{x})|_{\boldsymbol{\theta}=\boldsymbol{\theta}^*}$ and a stochastic f_{Init} following the NNGP.

Using the model defined in equation 2 and the training process described in equation 3, equation 1 effectively becomes:

$$\text{Var}_{f_{\text{Init}} \sim \mu_{\text{NNGP}}} [f_T(x; \theta | \text{Init} = f_{\text{Init}})], \quad (34)$$

where $f_T(x; \theta | \text{Init} = f_{\text{Init}})$ indicates a network trained via equation 3 by time T , with f_{Init} as initialization.

When we set $t_s = 0$ (the initialization time), the perturbation Δf will be applied to f_{Init} . Therefore, given a fixed initialization f_0 to perturb, Theorem 1 gives an upper-bound over a perturbation of the initialization functional:

$$\text{Var}_{\Delta f} [f_T(x; \theta | \text{Init} = f_0 + \Delta f)], \quad (35)$$

since \hat{f}_T is supposed to be trained from initialization $f_0 + \Delta f$, we have $\hat{f}_T = f_T(x; \theta | \text{Init} = f_0 + \Delta f)$, hence the above.

Comparing it to equation 34, we see that the difference between them is the distribution of the initialization functional f_{Init} . In equation 34, f_{Init} distributes according to the NNGP; while in equation 35, it is centered around f_0 with a stochastic perturbation Δf . Intuitively, by using theorem 1, we approximate the predictive variance trained from the NNGP prior with the predictive variance trained from a random perturbed initialization $f_0 + \Delta f$. Figure 2 visualizes such an approximation.

B Details of Experimental Setup

B.1 Dataset Descriptions

An overview of all considered datasets is provided below. ID and OOD dataset setups are summarized in Table 3. Please refer to [56] for more details.

ID Datasets

CIFAR-10 The CIFAR-10 training set [30] consists 60000 32×32 colored images, containing 10 classes of *airplane*, *automobile*, *bird*, *cat*, *deer*, *dog*, *frog*, *horse*, *ship* and *truck*. The test set originally contained 10000 images from the same classes, where we separated 1000 validation images and 9000 test images from the original test set following [56]. The dataset and each split are even in classes.

CIFAR-100 CIFAR-100 [30] contains 60000 32×32 images sampled from 100 classes, covering a wider range of images beyond CIFAR-10. Similar to CIFAR-10, 1000 images are taken out from the ID test set, forming a validation set.

ImageNet-1K ImageNet-1K [9], also known as ILSVRC 2012, spans 1000 object classes and contains 1,281,167 training images, 50,000 validation images and 100,000 test images, each of size 224×224 . In the OpenOOD setup, 45,000 validation images are used as ID test and 5,000 as ID validation.

ImageNet-200 ImageNet-200 [56] is a 200-class subset of ImageNet-1K compiled in OpenOOD version 1.5, with 10,000 224×224 validation images.

Semantic-Shift OOD Datasets

Tiny-ImageNet Tiny-ImageNet [33] has 100,000 images divided up into 200 classes, each with 500 training images, 50 validating images, and 50 test images. Compared to ImageNet-200, every image in Tiny-ImageNet is downsized to a 64×64 coloured image.

MNIST Modified National Institute of Standards and Technology database [34] contains 60,000 training and 10,000 test images of handwritten digits. Each image is anti-aliased, normalized and centered to fit into a 28×28 pixel bounding box.

SVHN Street View House Number [41] dataset contains house numbers that are captured on Google Street View, consisting of 73257 digits for training, and 26032 digits for testing. In our setup, we used the MNIST-like 32×32 format, centered around a single character.

Textures Describable Textures Dataset [7] is a set of 47 categories of textures, collected from Google and Flickr via relevant search queries. It has 5640 images, 120 images for each category, where the sizes range between 300×300 and 640×640 .

Places365 Places365 [57] is a scene recognition dataset. The standard version is composed of 1.8 million train and 36000 validation images from 365 scene classes.

NINCO No ImageNet Class Objects [4] consists of 5879 samples from 64 OOD classes. These OOD classes were selected to have no categorical overlap with any classes of ImageNet-1K. Each sample was inspected individually by the authors to not contain ID objects.

SSB-Hard Semantic Shift Benchmark-Hard [49] split contains 49,000 images across 980 categories of ImageNet-21K that has a short total semantic distance.

iNaturalist The iNaturalist dataset [48] has 579,184 training and 95,986 validation images from 5,089 different species of plants and animals.

OpenImage-O OpenImage-O [31] is image-by-image filtered from the test set of OpenImage-V3, which has been collected from Flickr without a predefined list of class names or tags. In the OpenOOD setup, 1,763 images are picked out as validation OOD.

Covariate-Shift OOD Datasets

Blur-ImageNet This blurred ImageNet dataset contains ImageNet images with a Gaussian blur of $\sigma = 2$. The same splits are used as in the above description in the ImageNet-1K section.

ImageNet-C ImageNet-C [22] has 15 synthetic corruption types (such as noise, blur, pixelate) on the standard ImageNet-1K, each with 5 severities. In OpenOOD, 10,000 images are randomly sampled uniformly across the 75 combinations to form the test set.

ImageNet-R ImageNet-R [21] contains 30,000 images of different renditions of 200 ImageNet classes, such as art, graphics, patterns, toys, and video games.

ImageNet-ES ImageNet-ES [3] consists of 202,000 photos of images from Tiny-ImageNet. Each image is displayed on screen with high fidelity and photographed in a controlled environment with different parameter settings. We only used the 64,000 photos in the test set.

B.2 Hyper-parameters

In practice, when handling hyperparameters, we found it beneficial to first search for an optimal value for J_{scaling} , the most important parameter of TULiP as pointed out in Sec . 5. It controls the overall strength of TULiP and may depends on the network architecture and training scheme. Another important parameter is ϵ , though it has relatively less impact as long as the perturbation is not overwhelming the network’s original weights. If one’s computational resource allows for further exploration, optimal values of λ and δ can be searched for better performance. Typically, when increasing δ , λ should be decreased as they have a multiplicative relationship. If a validation set is not available, one may either use the suggested value or investigate network outputs after weight perturbation. When the network output becomes senseless after perturbation (e.g., a prediction close to random-guessing), it often indicates that ϵ or J_{scaling} is too large.

Grid Search Table 4 lists the hyper-parameter search range for all considered methods on the validation set.

\sqrt{o} scaling of λ In practice, when the number of network output dimensions o varies, we found that a \sqrt{o} scaling of λ -term (D) works more consistently. This might be due to our choice of using the computationally friendly Frobenius norm in Theorem 1 instead of a tighter spectrum norm. It is further explained in the proof listed in Sec. A.3.

Table 3: ID, OOD and OOD-val dataset setups.

ID Dataset	near-OOD	far-OOD	near/far-OOD Validation	Cov-Shift	OOD
CIFAR-10	CIFAR-100 Tiny-ImageNet	MNIST SVHN Textures Places365	Tiny-ImageNet		
CIFAR-100	CIFAR-10 Tiny-ImageNet	MNIST SVHN Textures Places365	Tiny-ImageNet		
ImageNet-1K ImageNet-200	SSB-Hard NINCO	iNaturalist Textures OpenImage-O	OpenImage-O		Blur-ImageNet ImageNet-C ImageNet-R ImageNet-ES

Table 4: Hyper-parameter (available at evaluation time) search ranges.

Method	Hyper-parameters
MC-Dropout	N/A
MDS	N/A
MLS	N/A
EBO	Temperature: {1}
ViM	Dimension: {256, 1000}
ASH	Percentile: {65, 70, 75, 80, 85, 90, 95}
ODIN	Temperature: {1, 10, 100, 1000} Noise: {0.0014, 0.0028}
TULiP	J_{scaling} : {1.0, 1.25, 1.5, 1.75, 2.0}

Hardware Each of our experiments is conducted on a single-node machine using an NVIDIA A6000 GPU.

B.3 Time Complexity of TULiP

As listed in Algorithm 1, TULiP requires $\mathcal{O}(M)$ forward passes to evaluate a minibatch of test data. Compared to single-pass methods, such limitation renders TULiP ineffective despite its performance as shown in Sec. 5, since forwarding a network could be expensive as networks grow in size. Nevertheless, TULiP is not $\mathcal{O}(M)$ times slower than single-pass methods as forward evaluation is not the sole bottleneck of inferencing. Table 5 compares the wall-clock inference time of TULiP and EBO (a single-pass method) in our OOD setting.

Table 5: Wall-clock time of our OOD experiments, contains a serial sequence of inference on ID (top row) and all corresponding OOD datasets (near and far).

Method	Forward passes	CIFAR-10	ImageNet-200	ImageNet-1K
EBO	1	44.32s	112.37s	3m 12.60s
TULiP $\mathcal{O}(M)$, $M = 10$		96.30s (2.17x)	190.41s (1.69x)	10m 59.24s (3.42x)